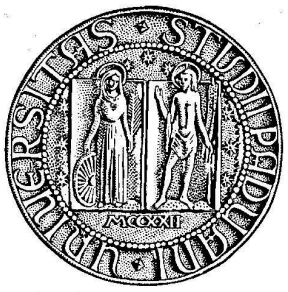

UNIVERSITÀ DEGLI STUDI DI PADOVA

FACOLTÀ DI SCIENZE MM. FF. NN.

Dipartimento di Geoscienze

Direttore Prof.ssa Cristina Stefani

TESI DI LAUREA MAGISTRALE IN GEOLOGIA E GEOLOGIA TECNICA

Exhumation Mechanisms in Hot Orogens: insight from numerical modelling

Relatore: Dott. Manuele Faccenda

Laureando: Andrea Piccolo

ANNO ACCADEMICO 2014/2015

-All right- said Deep Thought -The answer to the Great Question of Life, the Universe and Everything...Is... Fourty-two- said Deep Thought, with infinite majesty and calm.

— The Hitchhikers's Guide to the Galaxy, Douglas Adams

Contents

1 Introduction **9**

1.1 Main subject of thesis work 10

1.2 Hot orogens 10

1.3 Coupling between climate and tectonics 12

1.4 Aims of the thesis 13

2 Numerical Technique **15**

2.1 I2VIS 15

2.1.1 Marker-in-Cell Technique 17

2.2 Fundamental Equations 18

2.2.1 Conservation Equation 18

2.2.2 Rheological Model 23

2.2.3 Partial Melting 26

2.2.4 Boundary conditions 27

2.2.5 Transport Equation 30

2.3 Summary 32

3 Results **37**

3.1 Numerical Setup 37

3.1.1 Initial Geometry and Geotherm 38

3.1.2 $P-T-t$ path 41

3.2 Symmetric Orogenetic style 42

3.2.1 General Feature 42

3.2.2 Reference Model 44

3.2.3 Examination of the effect of the friction angle 48

3.3 Asymmetric Orogenetic style 51
3.3.1 General Feature 51
3.3.2 Reference Model 52
3.3.3 Surface Modelling 57

4 Discussion **71**
4.1 Limit of the simulation and future perspectives 71
4.1.1 Partial melting 71
4.1.2 Metamorphic reactions 72
4.1.3 Transport Equation 72
4.2 Asymmetric models as numerical analogue of Himalayan orogenetic belt 73
4.2.1 Basic geological background of Himalayan Range 73
4.2.2 Great Himalaya Sequence, Main Central Thrust and South Tibetan Detachment: exhumation model and evolution of the Himalayan system 76
4.2.3 Paradigm shift 82
4.2.4 Discussion of the simulation results 85

5 Conclusion **89**
5.1 Channel Flow necessary condition 90
5.2 Channel Flow and surface processes 90

Bibliography **97**

Abstract

Hot orogens are characterised by high temperatures and large dimensions. The temperature is related to the crustal thickness achieved during the evolution of the orogenetic system. The high temperature achieved by this kind of orogens is high enough to induce a pervasive and massive partial melting of the middle-upper crust. The partially melted rocks have a lower density and viscosity than the unmelted counterpart. The partially melted region that forms in the interior of the orogens affects the post collisional evolution of the orogen and affects the way in which the rocks exhume at the surface. The partially melted rocks self-organize in a hot channel that flows underneath the orogen, and affects large portions of the orogenetic system. Since this low viscosity channel has high mobility and it is highly sensitive to pressure changes, one of the most intriguing issues is to analyse if the changes of the topographic relief, due to the surface processes, affects the advection of the hot channel and therefore the exhumation patterns of the rocks. The best example of hot orogens is the Himalayan range in which there is abundant geological and geophysical evidence supporting widespread partial melting. The exhumation mechanism of the Great Himalayan Sequence (GHS) was one of the most important arguments of the Himalayan research in the last decades, and the models proposed have been based on the coupling between tectonics and climate. The most popular and predictive of these models was the channel flow model proposed by Beaumont [Beaumont et al., 2001] in which the GHS is interpreted as the coherent slice of Indian partially melted crust which has migrated from the Tibet, in the North, to the southern flank of the Himalayan range due to the established pressure gradient between the Tibetan plateu and the orogeny front. According to this model, the exhumation of the GHS is caused by the high and focused erosion in the souther flank. Recent researches have pointed out that the structural complexity of GHS

is incompatible with the channel flow model. The aim of this thesis work is to reproduce all the principal features of hot orogens by using numerical modelling in order to i) test the influence of the surface processes on the partially melted crust and on the exhumation patterns of the rocks, and ii) compare the simulation results with the observations from the Himalayan range in order to verify if the exhumation patterns predicted by the channel flow model is a inherent feature of hot orogens. Results show that partial melting in the mid-upper crust always forms, owing to the accreted highly radiogenic sediments and the thick orogenic crust. Different patterns of exhumation and metamorphism are reproduced, most of which are consistent with different exhumation models proposed. Additionally, the results of the simulations give other important insights: i) the focused erosion is not the necessary condition to the exhumation of the partially melted rocks and of the channel flow; ii) the shape of the channel flow is affected by the timing of the erosion; iii) the sedimentation rate have first order implication on the development of the orogens.

Chapter 1

Introduction

The orogenetic processes are complex: they are highly sensitive to the initial condition (geometry of the rock sequence, the rock properties, mantle heat flux...). For example, metamorphic reactions produce different kinds of rock with different mechanical properties, which may facilitate either the oceanic lithosphere or continental lithosphere subduction [Burov et al., 2014]. The initial geometry of the rocks or the variability of properties of the rock sequences may play a fundamental role for the development of the thrust sheet belt. This complexity cannot be completely reproduced by the numerical technique, but this does not imply that the information extrapolated from the simulation is not valid. Earth scientists have tried to reproduce the mechanical-chemical processes that build up the orogen by using a backward analysis and laboratory experimental data. This scientific method is valid and produces testable scientific hypotheses, but not all the geological problems can be easily handled without a forward analysis. The forward analysis is simply the extrapolation of the processes reproduced in laboratory to nature (for example the faulting of rock samples in laboratory). The main problem is that almost all of the geologic processes develop at geologic time scales and/or hundreds of kilometres below the surface. Despite the intrinsic shortcomings, numerical modelling provides crucial information, which can be used to better interpret nature. The numerical approach has no scientific meaning without a validation by field data; conversely, the interpretation of field data is not unique, for example it is difficult to reconstruct the evolution of convergent margins where different processes occur simultaneously. By using numerical modelling it is possible to test the various hypotheses, which

are constructed through the field work. On the other hand, the objectivity of the numerical modelling is not absolute, since the simulations are based on the arbitrary condition which we set, and we have to bear in mind the difference between forcing the reality to accommodate our models from the tentative to reproduce a natural process.

1.1 Main subject of thesis work

The main theme of the thesis is the burial and exhumation processes in hot orogens. My work is principally focused on the reproduction of a simulation that have all the characteristic features of hot orogens (and of the Himalayan range) and to verify how the surface processes may induce variations on the exhumation patterns or in the development of the orogen. The first section is the description of the concept of hot orogen, while the second section is a short review of the effects of the surface processes on the development of the orogens and on the exhumation processes.

1.2 Hot orogens

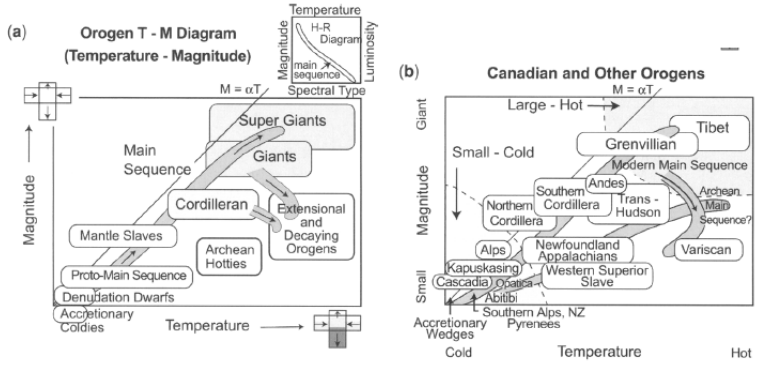

Fig. 1.1: T-M diagram: a) Classification diagram; b) Orogenetic system plotted in the diagram [Beaumont et al., 2006]

A hot orogen is an orogenetic system in which the crustal thickness and heat production is sufficiently high for the formation of a low viscosity partially melted zone in the orogens [Beaumont 2006, 2010]. This concept derives from the classification of the orogen based on the thermal state and thickness of the orogenetic system proposed by Beaumont [Beaumont 2006, 2010]. This classification is based on a diagram that is similar to the one proposed by Hertszprung-Russel for the classification

of the star [1]. The magnitude of the orogenetic system is plotted against the temperature achieved by it: magnitude is the ratio between the lithosphere thickness achieved by the orogenetic system and the normal non orogenetic lithosphere thickness; analoguosly, the temperature is expressed as a ratio between the thermal state of the orogenetic lithosphere and the non orogenetic lithosphere. The temperature is closely related to the magnitude of the orogens: the temperature increases with the magnitude, because, with depth, the thermal state emerges with the self-heating processes. The first relation that involves the two variables is the following:

$$M = \alpha T$$

where M is the magnitude of the orogen, T is the temperature, and α is the slope of the linear relation. As for the H-R diagram, it is possible to plot the evolutionary path of the orogen. Therefore the orogenetic system can be defined as a function of the evolutionary path, which depends on several features, for example the denudation rate and the radiogenic heat production [Beaumont et al., 2006, Beaumont et al., 2010]. The evolutionary path that can be traced by using the orogenetic system plotted in the T-M diagram is not linear, but it deflects upward or downward. This deflection is a consequence of the thermal conductivity processes (in the conduction equation there are quadratic therms) and the limit imposed by the gravitational force. Consequently all of the orogens plot below the M line. By using this diagram as a reference, it is possible to infer the deformation mechanism in the orogen. The viscosity diminishes with temperature and, by using this diagram, it is possible to predict if large scale partial melting occurs. The first distinction is between the small, cold orogens and the large, hot orogens:

1. Small, cold orogens: they plot in the lower left of the T-M diagram: the lithospheric thickness is too low to permit the temperature to increase enough to weaken the rocks; consequently in this kind of orogens there is no low viscosity partially melted crust. For example, the orogen that fit this definition, and plot in the lower left of the diagram, are: Southern Alps in New Zealand, the Alps and the Pyrenees;

[1] The absolute visual magnitude is plotted against the spectral type [Hertszprung, 1905, Russell, 1912]

2. Large Large, hot orogens: they plot in the upper right of the T-M diagram: the lithospheric thickness is sufficiently high to permit the temperature to increase due to the self-heating processes; consequently, a large crustal portion may be partially melted. The mobility of the partially melted rocks is high as for the sensitivity with respect to the variation of pressure: therefore changes in the topographic relief, or different distrubution of the elevation may cause a massive flow of the partially melted crust. The most important example of this category is the Himalayan-Tibetan orogenetic system.

The Himalayan range has all of the necessary features to be classified as a hot orogen: the temperature achieved by the rocks is high, and large portions of the continental crust underwent partial melting. The low viscosity channel is highly sensitive to the change of pressure. Beaumont performed several numerical experiments to demonstrate the relation between surface processes (monsoonal erosion) and mode of migration of the partially melted crust [Beaumont et al., 2001, Beaumont et al., 2004]. As the main aim of this thesis is to describe the exhumation processes in the hot orogens, the behavior of the partially melted crust has to be investigated. Consequently, as the simulations were performed with the aim to examinate the implications of the behavior of the partially melted region on the exhumation processes, this analysis must be done by considering surface processes such as focused (monsoonal) erosion.

1.3 Coupling between climate and tectonics

One of the most intriguing geological problematic to resolve is the relation between the surface processes and the development of the orogens. The problem can be splitted in two parts:

1. the coupling between climate and tectonics

2. the effect of the surface processes on the tectonics processes

The first issue is associated to the effects on the climatic system (which, in turn, control the surface processes). This question is not the first aim of this thesis project.

The second issue is associated to the effects of the surface processes on the geological structure. The surface processes can be regarded as a dynamical loading and unloading [Burov and Toussaint, 2007]. The erosion is a dynamic unloading and the sedimentation is a dynamic loading. From the theoretically point of view, erosion may induce a thrust reactivation: if the orogen is thickened the results is an increasing of the loading that acts on the thrust: therefore the thickening processes caused by the thrust have a negative feedback on the displacement on the thrust surface: the strength of the slip surface increases with the normal pressure acting on it [Burov and Toussaint, 2007]. Therefore the erosional processes may induce a sufficiently unloading to reactivate the thrust. On the other hand the sedimentation may provide sufficient weak material to promote the displacement of the thrust range [Burov and Toussaint, 2007]. Surface processes may affect lithospheric and sub-lithospheric processes; for example, they may promote the continental subduction or they may inhibit it [Burov and Toussaint, 2007, Burov et al., 2014]. Erosion may also affects the style of the incipient collisional processes [Gerya et al., 2008]. Erosion may promote uplift and consequently the exhumation processes [Chemenda et al., 2000]. In particular, the focused erosion induced by the monsoonal activity in the southern flank of the Himalayan is one of the most important arguments in several models. The channel flow proposed by Beaumont is based on the influence of the focused erosion on the partially melted low channel in the Himalayan range. In this models, erosion induces a gravitationally driven flow from the Tibet to the Himalayan range [Beaumont et al., 2001, Beaumont et al., 2004].

1.4 Aims of the thesis

The main aim of this thesis is to reproduce all of the features of the hot orogens and the mechanism of the exhumation in this particular class of orogenetic systems, and in particular to reproduce all the first order feature of the Himalayan range. Consequently, the first tests have been performed with the specific aim to reproduce all the first order feature of the Himalayan orogens. The second generation of simulations has been performed:

1. to test the sensibility of the low viscosity channel flow to the surface processes;

2. to verify if the burial and exhumation processes are affected by the channel flow;

3. to compare the results with the recent geological/geophysical observations related to the Great Himalayan Sequence.

The numerical code used for the simulation is I2VIS, this code is written in C language, and all the numerical experiments are performed by using the high-performance computer facilites at Cineca (Bologna).

Thesis Structure

- In chapter 2, the numerical technique used for the simulations is described. All the equation used are described in order to give a reference numerical framework.

- In chapter 3, the results of the simulations are presented. In the first part of the chapter the used numerical setup is described. In the second part of the chapter the representative simulations are described. The results are classified into two broad categories: Symmetric orogenetic style, and Asymmetric orogenetic style.

- Chapter 4 is divided in two main parts: the first part is a critical discussion about the numerical models limitations; the second part is the discussion of the results with respect to the Himalayan range.

- In chapter 5 is dedicated to the possible conclusions that can be inferred from my simulation.

Chapter 2

Numerical Technique

All the simulations presented in this work were performed using I2VIS, a 2D petrological-thermo-mechanical code developed by Taras V. Gerya and David A. Yuen [Gerya and Yuen, 2003]. I2VIS solves the conservation equation of mass, momentum and energy using a conservative finite difference scheme and non diffusive marker-in-cell technique in order to simulate multiphase flow [Moresi et al., 2003].

2.1 I2VIS

I2VIS is a coupled petrological-thermomechanical code. It is based on an Eulerian/Lagrangian primitive variable formulation combined with moving marker technique [Woidt, 1978]. All the scalar properties of the rocks and temperature field are ascribed to the Lagrangian markers initially distributed in a fine regular mesh [Gerya and Yuen, 2003].

The Eulerian grid is rectangular, irregular and fully staggered (fig.2.1). These grid properties are useful for two reasons:

1. resolution of Partial Difference Equation (PDE) is more accurate [1];
2. irregular grids are useful for handling geodynamic problems, because it is possible to use high resolution in particular zone of the numerical domain and near grid's boundary to minimize numerical fluctuactions [Fornberg, 1998].

All the marker properties are interpolated to the nodes of the Eulerian grid by

[1] accuracy of fully staggered grid is four time higher [Fornberg, 1998]

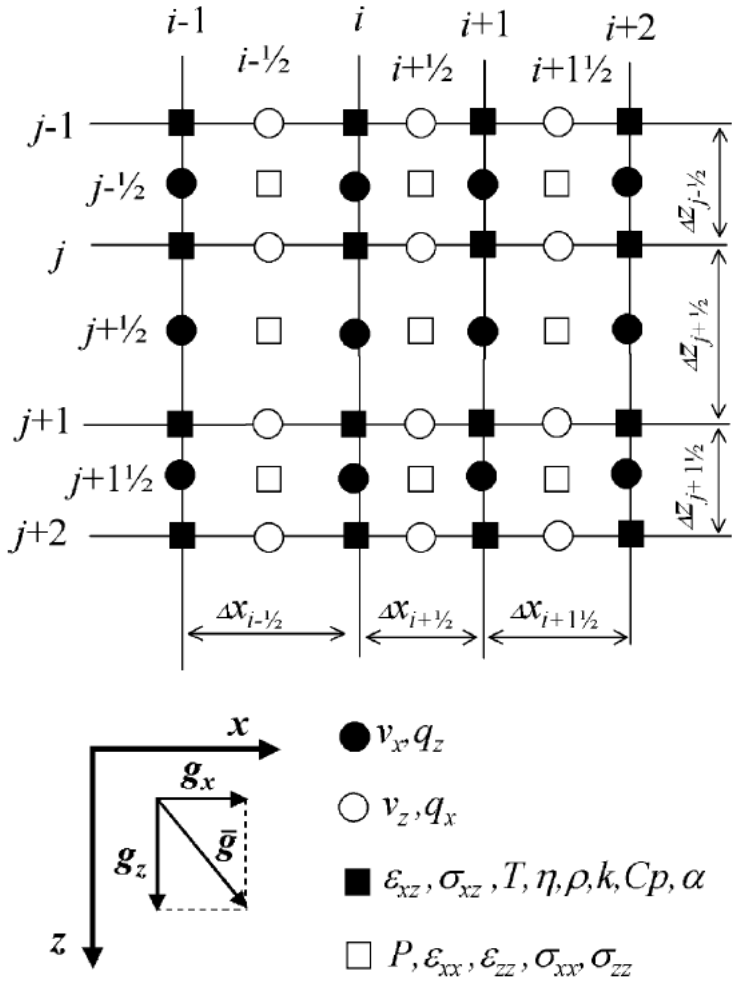

Fig. 2.1: Schematic rappresentation of the used Eulerian staggered grid used. g_x and g_z
are respectively the horizontal and vertical components of the gravitational acceleration. There are four types of node. Each type of node is associated with specific physical properties (e.g. the nodes, indicated by black fill square symbol, are associated to T, η, ρ, k, C_p and α) [Gerya and Yuen, 2003]

using a bilinear interpolation scheme with first order in accuracy which is numerically unconditional stable [2]. In contrast higher order schemes of interpolations are numerically unstable [Fornberg, 1998, De Smet et al., 2000].

I2VIS numerically solves the fundamental equation of the continuum mechanics in the Eulerian reference grid. All the equations are discretized following an arbitrary order in accuracy scheme combined with control volume method[3] [Fornberg,

[2]**Stability**: The numerical solution method is stable if the errors, that may appear during the solution process, are not magnified [Ismail-Zadeh and Tackley, 2010]

[3]**Control Volume Method**: Numerical domain is subdivide into several subdomain in which all the conservation equations are solved. The main advantages of the method is that, for any

1998,Patankar, 1980]. In order to conserve all the scalar, vectorial and tensorial variables, a conservative discretization scheme is used, which permits to avoid unrealistic numerical fluctuation [Gerya and Yuen, 2003, Gerya, 2009]. All the equations will be described in detail in Section 2.2.1. After solving all the conservation equations, lagrangian particles can be advected in space. I2VIS uses a fourth order in space and first order in time Runge-Kutta advection scheme [Gerya and Yuen, 2003,Gerya, 2009].

2.1.1 Marker-in-Cell Technique

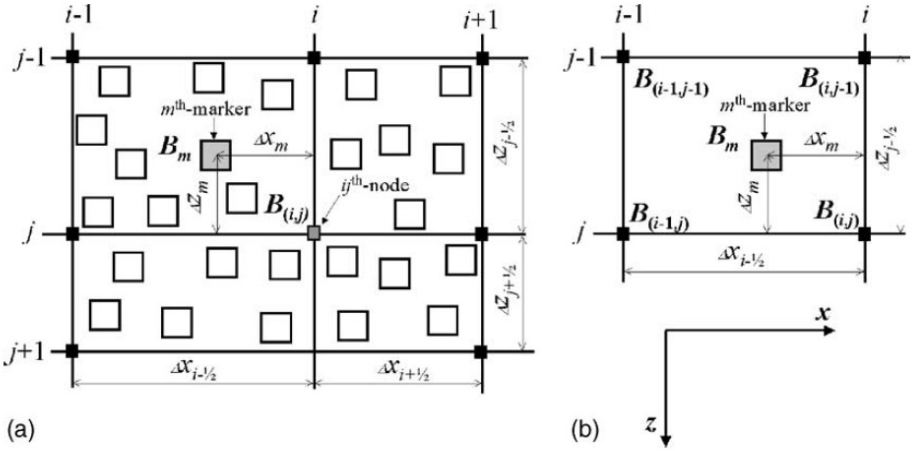

Fig. 2.2: This is a schematic representation of the bilinear interpolation scheme. In each eulerian grid cell there are several marker. Each marker has got its own statistical weight, which can be calculated from the normalized distance between the consider marker and the consider eulerian node. [Gerya and Yuen, 2003]

Marker-in-cell technique displays numerous computational advantages. Lagrangian particles store all the non-diffusive physical properties including the temperature field, which is a diffusive physical variable. At each time step, all the physical properties are interpolated from the marker into Eulerian Grid nodes using a bilinear interpolation scheme:

$$B_{(i,j)} = \frac{\sum_m B_m \; w_{m(i,j)}}{\sum_m \; w_{m(i,j)}} \tag{2.1}$$

group of control volume, all the solutions are conserved [Patankar, 1980]

$B_{i,j}$ is the interpolate value of the physical property considered at the $(i,j)^{th}$ eulerian node; B_m is the value of the property at the m^{th} marker, $w_{m(i,j)}$ is the marker m^{th}'s statistical weight at the $(i,j)^{th}$ node, calculated using average normalized distance between considered marker and eulerian node (fig.2.2) [Gerya and Yuen, 2003, Gerya, 2009].

The main advantages of the method of MIC is that it minimizes numerical diffusion due to advection. This approach to solves the advection equation can be also applied to the temperature field. In I2VIS is implemented an alghoritm that permits to minimize the numerical oscillation of the temperature. This alghoritm is based on the *Characteristics method* [4] proposed by [Malevsky and Yuen, 1991], which is modified in order to follow a resolution scheme similar to the advection of the field properties.

2.2 Fundamental Equations

2.2.1 Conservation Equation

Conservation of Mass

The equation describing conservation of mass or Continuity Equation, is a fundamental mathematical law in continuum mechanics. The physical principles behind this equation are simple: the mass of a body is invariant [Mase and Mase, 2010]. In other words for a given fixed volume, the mass variation in time is equal to the difference between the in-flux and out-flux of the mass. Continuity equation for a fixed volume has the following form:

$$\frac{\partial\, \rho}{\partial\, t} + \nabla(\rho\ \overrightarrow{v}) = 0 \tag{2.2}$$

where ρ is the local density, $\overrightarrow{v}$ is the local velocity vector. All the simulations presented in these work are bidimensional, thus the continuity equation has this general form:

[4] **Characteristics**:or characteristic curves are curve along which PDE can be solved as if it were an Ordinary differential Equation [Ismail-Zadeh and Tackley, 2010]. The method of the characteristics is based on these curves.

$$\frac{\partial v_x}{\partial x} + \frac{\partial v_z}{\partial z} = -\frac{1}{\rho}\frac{\mathbf{D}\rho}{\mathbf{D}t} \tag{2.3}$$

Equation 2.3 is the continuity equation for compressible media [Gerya and Yuen, 2007]. v_x is local velocity component along x axis of the cartesian reference system, v_z is the local velocity component along z axis, ρ is local density, $\frac{\mathbf{D}}{\mathbf{D}t}$ is substantive time derivative. In the absence of melt segregation or phase transformation the geological continuum media can be considered incompressible, therefore the continuity equation can be written as:

$$\frac{\partial v_x}{\partial x} + \frac{\partial v_z}{\partial z} = 0 \tag{2.4}$$

This equation is discretized following a first order in accuracy scheme.

Conservation of momentum

Conservation of momentum is described by the momentum equation. The Momentum equation is the mathematical formulation of the *principle of linear momentum*: the variation in time of the linear momentum of a body is equal to the forces acting on it (external or internal forces) [Mase and Mase, 2010]:

$$\frac{\partial \sigma_{i,j}}{\partial x_j} + \rho \mathbf{g}_i = \rho \left(\frac{\partial v}{\partial t} + \left(v_j \frac{\partial v_j}{\partial x_j} \right) \right) \tag{2.5}$$

$\frac{\partial \sigma_{i,j}}{\partial x_j}$ is partial derivate in space of the component of total stress tensor acting along x_j, ρ is density; $\mathbf{g}_i$ is gravity acceleration along the given direction, i and j are coordinate indexes(x,z). The right side of the equation is the inertial term.

The total stress tensor must be decomposed into its deviatoric part and isotropic components:

$$\frac{\partial \sigma'_{i,j}}{\partial x_j} + \rho \mathbf{g}_i - \frac{\partial \mathbf{P}}{\partial x_i} = \rho \left(\frac{\partial v}{\partial t} + \left(v_j \frac{\partial v_j}{\partial x_j} \right) \right) \tag{2.6}$$

$\sigma'_{i,j}$ is the deviatoric stress tensor,$\frac{\partial \mathbf{P}}{\partial x_i}$ is the pressure gradient along the considered direction. [5]

On geological timescales rocks behave as highly viscous fluid. This rheological behaviour has two important implications:

[5]Pressure is the isotropic component of total stress tensor.

1. the Navier-Stokes equation can be simplified to the Stokes equation of slow motion, because the inertial term becomes negligible in highly viscous fluids, and can be dropped out:

$$\frac{\partial \sigma'_{i,j}}{\partial x_j} - \frac{\partial \mathbf{P}}{\partial x_i} = -\rho \mathbf{g}_i \tag{2.7}$$

2. The newtonian law of friction can be used in order to link the deviatoric stress tensor to the deviatoric strain rate tensor:

$$\sigma'_{i,j} = 2\eta \left(\dot{\epsilon}'_{i,j} - \frac{1}{3}\delta_{i,j}\dot{\epsilon}_{kk} \right) \tag{2.8}$$

where η is the viscosity ($\mathrm{Pa{\cdot}s^{-1}}$), $\dot{\epsilon}_{i,j}$ is the total strain rate tensor; $\delta_{i,j}$ is Kronecker's delta, which is equal 1 if i=j and 0 if i≠j, $\dot{\epsilon}_{kk}$ is the isotropic component of total strain rate tensor.

The components of the strain rate tensor can be derived from the velocity field:

$$\dot{\epsilon}_{i,j} = \frac{1}{2} \left(\frac{\partial v_i}{\partial x_j} + \frac{\partial v_j}{\partial x_i} \right) \tag{2.9}$$

The costitutive relationship between deviatoric stress and deviatoric strain rate is:

$$\sigma'_{i,j} = 2\eta \dot{\epsilon}'_{i,j} \tag{2.10}$$

From equation 2.7, the set of 2D Stokes equation used by I2VIS is:

$$\frac{\partial \sigma'_{xx}}{\partial x} + \frac{\partial \sigma'_{xz}}{\partial z} - \frac{\partial P}{\partial x} = 0 \tag{2.11}$$

$$\frac{\partial \sigma'_{zz}}{\partial z} + \frac{\partial \sigma'_{zx}}{\partial x} - \frac{\partial P}{\partial z} = -\rho(C, P, T, M)\mathbf{g}_z \tag{2.12}$$

g_x is equal to zero, so the right term of the (2.11) can be dropped out. $\rho(T, P, C, M)$ is density which varies as a function of temperature, pressure, composition and volumetric degree of melting, the density variation due to the partial melting is described in section 2.2.3. Sub-solidus density is calculated as :

$$\rho(P,T,C) = \rho_0(C)[1-\alpha(T-T_0)][1+\beta(P-P_0)] \tag{2.13}$$

$\rho_0(C)$,P_0 and T_0 are respectively the density and pressure and temperature value at the standard conditions, α is the thermal expansion and β is the compressibility. [Gerya and Burg, 2007]

Continuity equation and 2D Stokes equation must be solved togheter. The solution of these equations are the global velocity field and the pressure field. From the velocity field is possible to find all the deviatoric stress components and the strain rate components.

Conservation of Energy

Heat is transferred from a region of space to another by conductive or advective processes. The temperature evolution of a given fixed volume in space is linked to its internal heat production and to the difference between the in-flux and out-flux. The equation of the conservation of energy is solved in the Eulerian grid using the implicit formulation:

$$\rho C_p \left(\frac{DT}{Dt}\right) = -\frac{\partial q_x}{\partial x} - \frac{\partial q_z}{\partial z} + H_r + H_a + H_s + H_l \tag{2.14}$$

$$\frac{\partial q_x}{\partial x} = -k(T,P,C)\frac{\partial T}{\partial x} \tag{2.15}$$

$$\frac{\partial q_z}{\partial z} = -k(T,P,C)\frac{\partial T}{\partial z} \tag{2.16}$$

where C_p is heat capacity, q_x and q_z are respectively heat flux along x direction and z direction. $k(T,P,C)$ is thermal conductivity coefficient which varies according to this empirical law [Clauser and Huenges, 1995]

$$k(T,P,C) = \left(k_1 + \frac{k_2}{T+0.77}\right) exp(k_3 P) \tag{2.17}$$

where k_1,k_2 and k_3 are empirical parameters specific for each rock type.

H_s and H_a are calculated after the solution of continuity and Stokes equations.

Boussinesq approximation [6] is extended for both equation:

Adiabatic heating is consumption or release of heat due to variation of the pressure.

$$H_a = T\alpha \left(v_x \frac{\partial P}{\partial x} + v_z \frac{\partial P}{\partial z} \right) \tag{2.18}$$

Viscous shear heat is the production of heat due to the internal friction of the fluid.Its role in the geodinamic processes is demonstrated by [Burg and Gerya, 2005].

$$H_s = \sigma'_{xx}\dot{\epsilon}_{xx} + \sigma'_{zz}\dot{\epsilon}_{zz} + 2\sigma'_{xz}\dot{\epsilon}_{xz} \tag{2.19}$$

Radiogenic elements produce heat. Each type of rock has a specific range radiogenic of heat production values [Turcotte and Schubert, 2014]. H_r is assumed to be a costant value that depends on composition.

$$H_r = cost(C) \tag{2.20}$$

Latent heat, H_l contribution due to melt/solid equilibrium is included implicity by increasing C_p and α [Gerya and Burg, 2007, Faccenda et al., 2008]

$$C_p^{eff} = C_p + Q_l \left(\frac{\partial M}{\partial T} \right)_P \tag{2.21}$$

$$\alpha^{eff} = \alpha + Q_l \left(\frac{\partial M}{\partial P} \right)_T \tag{2.22}$$

C_p^{eff} is the heat capacity calculated taking into account melt/solid equilibrium, α^{eff} is thermal expansion coefficient calculated taking into account melt/solid equilibrium, Q_l is latent heat of the reaction, M is volumetric degree of melting.

[6] **Boussinesq approximation**: the density variation in the conservation energy equation are neglected since they are small. [Ismail-Zadeh and Tackley, 2010].

2.2.2 Rheological Model

I2VIS uses a composite visco-plastic rheological model based on deformation invariant [Ranalli, 1995]. The total second invariant strain is:

$$\dot{\epsilon}'_{II} = \dot{\epsilon}_{vis} + \dot{\epsilon}_{pl} \tag{2.23}$$

where $\dot{\epsilon}_{vis}$ is the contribution of viscous deformation processes and $\dot{\epsilon}_{pl}$ is the contribution of plastic deformation processes.

Firstly I introduce all the viscous creep law and then the plastic flow rule.

Viscous creep laws

There are two viscous deformation mechanisms: diffusion and dislocation creep. Diffusion creep mechanism is newtonian because stress and strain rate have linear dependency on eachother, and the effective viscosity, for a given pressure and temperature condition, is costant and indipendent from stress and strain rate; Dislocation creep is non newtonian since stress and strain rate do not show linear dependencies therefore the viscosity depends on both applied stress and strain rate. Both mechanisms are always active,therefore effective viscosity is calculated as harmonic summation between viscosity derived from each mechanism:

$$\frac{1}{\eta_{eff}} = \frac{1}{\eta_{diff}} + \frac{1}{\eta_{disl}} \tag{2.24}$$

where η_{eff} is effective viscosity; η_{diff} is diffusion creeps viscosity and η_{disl} is dislocation creep's viscosity.

I2VIS computes only the dislocation creep law, from which it derives diffusion creep viscosity.

$$\eta_{disl} = \frac{\sigma'_{II}}{2\dot{\varepsilon_{II}}} = \frac{1}{2}\, A_D \sigma'^{1-n}_{II} exp\left(\frac{E_{att} + P \cdot\ V_{att}}{RT}\right) \tag{2.25}$$

where σ'_{II} and $\dot{\epsilon}'_{II}$ are respectively second invariant of deviatoric stress and stran rate tensors, A_D, E_{att} and V_{att} are respectively the pre-exponential factor,activaction energy and activaction volume, while n is stress exponential factor; R is the gas constant.

Diffusion creep is a thermally activated mechanism, and it is the most convenient way to accomodate deformation at low stress conditions, while the other one is dominant for high stress levels. An useful concept to introduce is stress transition, τ_{trans} which is the value of the second invariant of the deviatoric stress tensor at which diffusion creep viscosity has the same value of the dislocation creep viscosity, τ_{trans} ,defines the transition from dominant diffusion creep mechanism to dominant dislocation creep mechanisms [Turcotte and Schubert, 2014] :

$$\eta_{diff} = \frac{1}{2}\ A_D \tau_{trans}^{1-n} exp\left(\frac{E_{att} + P \cdot\ V_{att}}{RT}\right) \tag{2.26}$$

Therefore η_{diff} can be linked to $\eta_{disl}$by stress transition.E_{att} A_D and V_{att} are assumed to be the same for both processes. The stress transition is chosen as costant value. Since these simplifications are used, for given values of temperature and pressure, the ratio between η_{diff} and η_{disl} is:

$$\frac{\eta_{diff}}{\eta_{disl}} = \left(\frac{\sigma'_{II}}{\tau_{trans}}\right)^{n-1} \tag{2.27}$$

equation 2.27 can be rearranged as:

$$\eta_{diff} = \eta_{disl}\left(\frac{\sigma'_{II}}{\tau_{trans}}\right)^{n-1} \tag{2.28}$$

The value of the τ_{trans} is important, because it indirectly controls rocks' strenght. Low τ_{trans} values make the rocks stronger [Gerya and Stöckhert, 2006, Faccenda, 2014]. In the simulation performed during this thesis project, stress transition has had a fundamental role.

Plastic Yielding Criterion

The strenght is limited by imposing a plastic yielding criterion.The effective creep viscosity for plastic behaviour can be computed as:

$$\eta_{brit} = \frac{\tau_{yield}}{2\dot{\epsilon}'_{II}} \tag{2.29}$$

where η_{brit} is plastic creep viscosity upper limit, τ_{yield} is the yield stress value. Yield stress is computed with a Drucker˘Prager criterion [Ranalli, 1995]:

$$\tau_{yield} = ccos(\phi_{dry}) + sin(\phi_{dry})P(1-\lambda) \tag{2.30}$$

c is rock's cohesion, P is pressure,ϕ is frictional angle, P is pressure, and lambda is the lambda factor:

$$\lambda = \frac{P_f}{P_L} \tag{2.31}$$

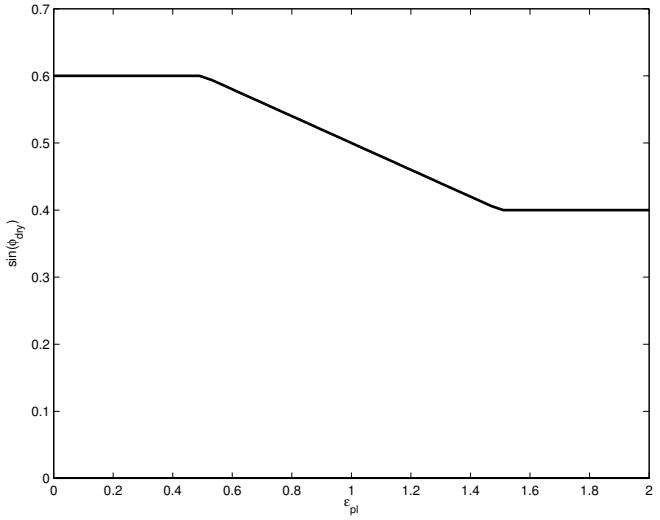

Fig. 2.3: This an example of the variation of frictional angle due to weakening process $sin(\phi_{dry})$

Rocks show a complex behavior even for plastic rheology. During deformation processes rocks can be weakened by deformation itself, or by other chemical and physical processes. For example in natural context faults are zone of high permeability, consequently fluids can be induced to pass through fault zones; fluids are reactive, so they can induce chemical reactions which weakens rock's frictional properties [Wibberley et al., 2008, Wintsch et al., 1995]. Even if these behaviors are complicated to be realistically modeled , the first order consequence of weakening processes can be simulated using a simplified mathematical models. In I2VIS these processes are implemented following these conditions:

$$\begin{cases} \epsilon < \epsilon_0 \mapsto a = a_0 \\ \epsilon_0 < \epsilon < \epsilon_1 \mapsto a = a_0 + (a_0 - a_1)\left(\dfrac{\epsilon - \epsilon_0}{\epsilon_1 - \epsilon_0}\right) \\ \epsilon > \epsilon_0 \mapsto a = a_1 \end{cases} \tag{2.32}$$

a can be either the frictional angle or the cohesion. a_0 and a_1 are respectively the initial value and the final value of the property considered. After plastic failure, rock starts to deform plastically,and as soon as ϵ_{pl} reaches a particular value (ϵ_0), a begins to change, following a linear relationship defined by using two arbitrary value of the strain ϵ_0 and ϵ_1. The weakening process stops when the plastic deformation reaches ϵ_1 and a is equal to a_1. (see fig.2.3)

2.2.3 Partial Melting

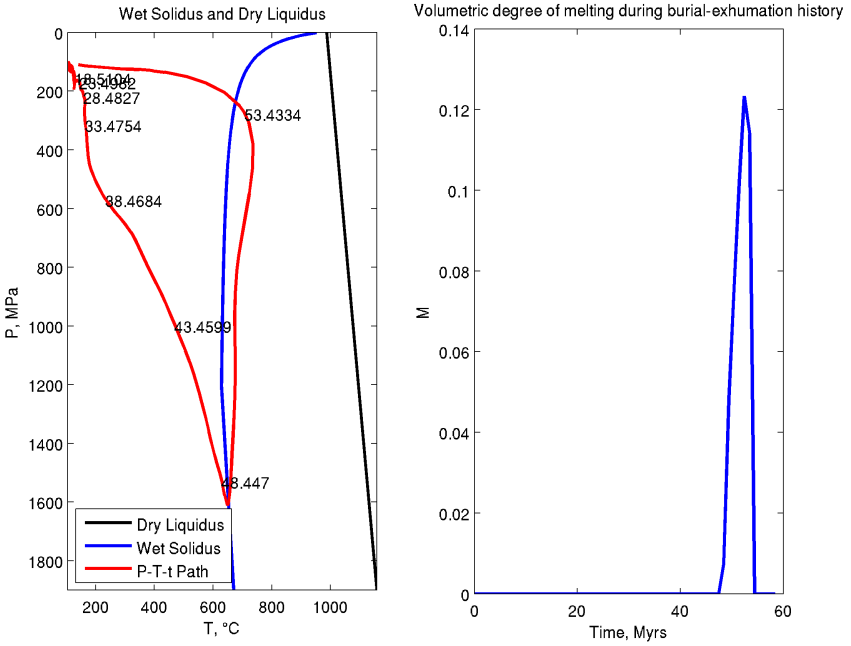

Fig. 2.4: Left: P-T space in which the parametrized dry liquidus and wet solidus of the upper crust are plotted toghether example of synthetic P-T-t path for a lagrangian particle. Right: the volumetric degree of melt evolution vs time is plotted for the same lagrangian particle.

Partial melting is a fundamental process which has to be taken into account in order to realistically simulate orogenic processes. Density and viscosity of the

melt bearing rocks are lowered than their dry counterparts thus their mobility and positive buoyancy significantly augment. The way in which this process has been implemented in I2VIS is relatively simple. Each rock type has its own dry liquidus and wet solidus function[7] and M (volumetric degree of melting) as [Gerya and Burg, 2007, Faccenda et al., 2008](see fig.2.4):

$$M = \begin{cases} M = 0 \mapsto T < T_s \\ M = \dfrac{T - T_s}{T_l - T_s} \mapsto T_s \leq T \leq T_l \\ M = 1 \mapsto T > T_l \end{cases} \tag{2.33}$$

where T_l and T_s are respectively temperature of the wet solidus and dry liquidus for a given value of pressure. As it was mentioned before, partial melting affects rocks rheology, this effect is described by [Gerya and Burg, 2007, Faccenda et al., 2008]:

$$\eta = \eta_0 exp\left(2.5 + (1 - M)\left(\frac{1 - M}{M}\right)^{0.48}\right) \tag{2.34}$$

η_0 is an empirical parameter, different for any rock type. Density changes according to:

$$\rho^{eff} = \rho_{solid} - M(\rho_{solid} - \rho_{liquid}) \tag{2.35}$$

where ρ^{eff} is effective density, ρ_{solid} is rock density, ρ_{liquid} is melt density.

As it was mentioned in section 2.2.1, the latent heat of the melting reaction is implicitly calculated in equation2.21 and in equation 2.22.

2.2.4 Boundary conditions

In order to solve the PDE equation it is necessary to define a set of boundary condition for the fundamental equation. The boundary conditions have a fundamental role in determining the intrinsic behavior of the simulation, therefore it is necessary to use the proper boundary conditions for the specific geodynamic problems which have to be investigated.

The numerical domain, in which all the calculations were performed, is rectangular. The boundary conditions for the solution of the continuity equation and

[7] see Tab. 2.1

Material	ρ_0 $kg\ m^{-3}$	k $Wm^{-1}K^{-1}$	$T_{wet\ solidus}$ K	$T_{dry\ liquidus}$ K	Q_l $\mathrm{kJ}m^{-3}$	H_r μWm^3	Flow Law
Upper Crust Sediments	Solid_{UC}: 2800 Melt_{UC}: 2400 Solid_S:2600 Melt_S:2400	$0.64 + \frac{807}{T+77} exp(4 \cdot 10^{-6} P)$	$P < 1200$ MPa $889 + \frac{17900}{P+54} + \frac{20200}{(P+54)^2}$ $P > 1200$ MPa $831 + 0.06P$	$1262 + 0.09P$	300	$1 - 5$	*Wet Quarzite*
Lower Crust	Solid: 3000 Melt: 2900	$1.18 + \frac{474}{T+77} exp(4 \cdot 10^{-6} P)$	$P < 1600$ MPa $974 - \frac{70400}{P+354} + \frac{77800000}{(P+354)^2}$ $P > 1600$ MPa $935 + 0.0035P + 0.0000062P^2$	$1423 + 0.105P$	380	0.25	*Mafic Granulite PlagioclaseAn75*
Oceanic Crust	Solid: 3000 Melt: 2900	$1.18 + \frac{474}{T+77} exp(4 \cdot 10^{-6} P)$	$P < 1600$ MPa $974 - \frac{70400}{P+354} + \frac{77800000}{(P+354)^2}$ $P > 1600$ MPa $935 + 0.0035P + 0.0000062P^2$	$1423 + 0.105P$	380	0.25	*PlagioclaseAn75*
Mantle	Solid: 3300	$0.73 + \frac{1293}{T+77} exp(4 \cdot 10^{-6} P)$	$\cdots$	$\cdots$	$\cdots$	0.022	*Dry Olivine*

Tab. 2.1: Rock Properties

2D Stokes equation are *free slip* for all sides of the numerical domain, except for the lower one, which has a *permeable boundary* condition. A free slip boundary condition implies that, at the grid boundary nodes, all the velocities orthogonal to the boundary are equal to zero(see equations 2.36) while the velocities components parallel to the boundary must not to vary in the direction normal to it. Permeable boundary or infinity like boundary condition is a particular way to express a free slip boundary condition: the free slip boundary condition is externally defined and the lower boundary of the eulerian grid behaves as a permeable membrane in which flow occurs in both direction (upwards and downwards) (see equation (2.37)).The following equation are the mathematical definition of all the boundary condition for the boundary orthogonal to x axis [Gerya, 2009]:

$$Free\ Slip_{\perp x} = \begin{cases} v_x = 0 \\ \dfrac{\partial v_z}{\partial x} = 0 \end{cases} \tag{2.36}$$

while the infinity like free slip is orthogonal to z axis and its formulation is:

$$Permeable\ Boundary_{\perp z} = \begin{cases} \dfrac{\partial v_z}{\partial z}\Delta L + v_z = 0 \\ \dfrac{\partial v_x}{\partial z} = 0 \end{cases} \tag{2.37}$$

where ΔL is the distance between the real grid boundary and the external boundary in which the free slip condition is applied.

The boundary condition for the conservation of energy equation are constant temperature in the upper boundary, symmetry for the right and left boundary and an *infinity like external constant temperature boundary condition* for the lower one. A symmetry boundary condition implies that there is not heat flux across the boundary (insulating boundary condition); constant temperature boundary condition simply means that the temperature along the given boundary is constant. An infinity like external constant temperature is similar to the mechanical counterpart, in that the constant temperature is externally defined [8]. The boundary condition equation are:

$$T = const(x, z, t) \tag{2.38}$$

[8]The temperature gradient between the actual boundary and the 'false' one is constant

$$Infinity\ like\ BC \begin{cases} T_{external} = const(x,z,t) \\ \dfrac{\partial T}{\partial z} = \left(\dfrac{T - T_{external}}{\Delta L}\right) \end{cases} \tag{2.39}$$

$T_{external}$ is the constant temperature defined for the external boundary.

$$Symmetry\ BC_x = \frac{\partial T}{\partial x} = 0 \tag{2.40}$$

A fixed v_x is prescribed in a narrow zone of the domain in order to simulate convergence. This v_x is fixed and do not vary in time. Since the convergence rate may cause intraplate stress and deformation, it is necessary to impose a low viscosity zone near the left boundary. This narrow zone of low viscosity allows the continental plate to be displaced without having any internal deformation until it reach the collisional zone.

2.2.5 Transport Equation

Variable	**Symbol**
z_{eros}	Erosion Level (m)
v_e	Erosion velocity $\left(\frac{mm}{s}\right)$
κ_e	Erosion coefficient $\left(\frac{1}{s}\right)$
κ_{mon}	Monsoonal erosion factor
t_{mon}	Time of monsoon enanched erosion *(Myrs)*
s_{sed}	Sedimentation level m
v_s	Sedimentation velocity$\left(\frac{mm}{s}\right)$
κ_S	Sedimentation coefficient $\left(\frac{1}{s}\right)$
ϑ_{max}	Maximum slope

Tab. 2.2: This is the table of the variables used for the surface processe. There is a variable that is not described in text: ϑ_{max} is the maximum slope. After calculating the erosion and the sedimentation effect to topography, I2VIS modifies the slope in according to the maximum slope possible.

The upper boundary has a free slip boundary. This boundary condition cannot simulate the evolution of the topography. In order to simulate topographic evolution, in all the simulation, the 'Sticky Air Approximation' is used:in the uppermost part of the numerical domain, there is a layer of low density and viscosity material, just like water or air. This layer transmit stress negligible to the part of the numerical domain of interest. Using this approximation it is possible to simulate topography

evolution without affecting the accuracy of the calculation [Crameri et al., 2012].

The evolution of the topography due to the surface processes may have an important role during the collisional processes [Avouac and Burov, 1996]. Topography can be considered as a loading function. The spatial variation of the topography may produce a *lower crust* flow due to pressure difference and the variation of the topography in time produces an isostatic response [Burov and Toussaint, 2007], this may produce a different behaviour of the crustal mantle interface during collision [Gerya et al., 2008]. During continental collision, surface processes induce a variation of loading in time and space, which produces different responses of the crust. For example erosion may induce a thrust reactivation, while sedimentation helps the under thrusting processes [Burov and Toussaint, 2007]. In order to realistically simulate collisional process, it is necessary to take into account the surface processes.

In I2VIS, the transport equation is used to simulate the topographyc evolution [Crameri et al., 2012, Faccenda et al., 2008]:

$$\frac{\partial z_{es}}{\partial t} = v_z - v_x \left(\frac{\partial z_{es}}{\partial x} \right) - v_s + v_e \tag{2.41}$$

where $\frac{\partial z_{es}}{\partial t}$ is the time derivative of topography elevation in time;v_z and v_x are respectively the vertical component and the horizontal component of the velocity field at the surface; $\frac{\partial z_{es}}{\partial x}$ is the partial derivative along x direction; v_e and v_s are respectively erosion and sedimentation velocity.

$$\begin{cases} if z_{es} < z_{eros} \mapsto v_e = 0.3156 \frac{mm}{yrs} \\ if z_{es} > z_{sed} \mapsto v_s = 0.1578 \frac{mm}{yrs} \end{cases} \tag{2.42}$$

$z_{erosion}$ and $z_{sedimentation}$[9] are respectevely the z coordinate below which erosion and above which sedimentation take place.[10]. V_e and V_s values are examples, these parameter are frequently changed in the test performed.

It is also implemented a topography dependent erosion and sedimentation velocities:

[9] the value of $z_{erosion}$ and $z_{sedimentatio}$ will be shown in the Results chapter.

[10] NB: the z coordinate is positive downward

$$V_e = v_e + \kappa_e(z_{eros} - z_{es}) \tag{2.43}$$

$$V_s = v_s + \kappa_s(z_{es} - z_{sed}) \tag{2.44}$$

κ_e and κ_s are erosion and sedimentation coefficent, that control how much erosion and sedimentation velocities increase with the topography.

Topographic evolution due to tectonic processes is described using the velocity field at the air/water-rock interface. After the calculation of the tectonic topographic response, the surface processes are applied to the topography. All the necessary variable used to calculate the transport equation are listed in Tab. 2.2.

As it was mentioned, the evolution of the topography may play an important role during continental collision. Surface processes are the expression of the climate. Orogenetic processes modify the atmospheric circulation which implies that climate may locally or globally change during the mountain building process. Climate changes due to tectonic processes could have played an important role during the evolution of the Himalaya orogenic belt, since the topography acted as natural barrier for the Monsoon [Thiede and Ehlers, 2013]. In order to achieve the best possible representation of the Himalaya tectonic evolution and test the hypothesis of the coupling between tectonics and surface processes, it is necessary to model the monsoon erosional effect in the southern margin of the Himalaya.Consequently, Moonsonal erosion is defined in the area limited by the trench and the adjacent max elevation of the topographic relief:

$$if\ t > t_{mon} \mapsto v_{e\ mon} = \kappa_{mon} v_e \tag{2.45}$$

t_{mon} is the time in which monsoon enanched erosion starts; $v_{e\ mon}$ is the new erosion velocity; κ_{mon} is a multiplicative factor applied to the basic v_e.

2.3 Summary

All the conservation equations and the other equations are solved by I2VIS with a specific order. In order to contextualize all the equations described in the previous section, a short description of the code structure is introduced (see fig 2.5 for a

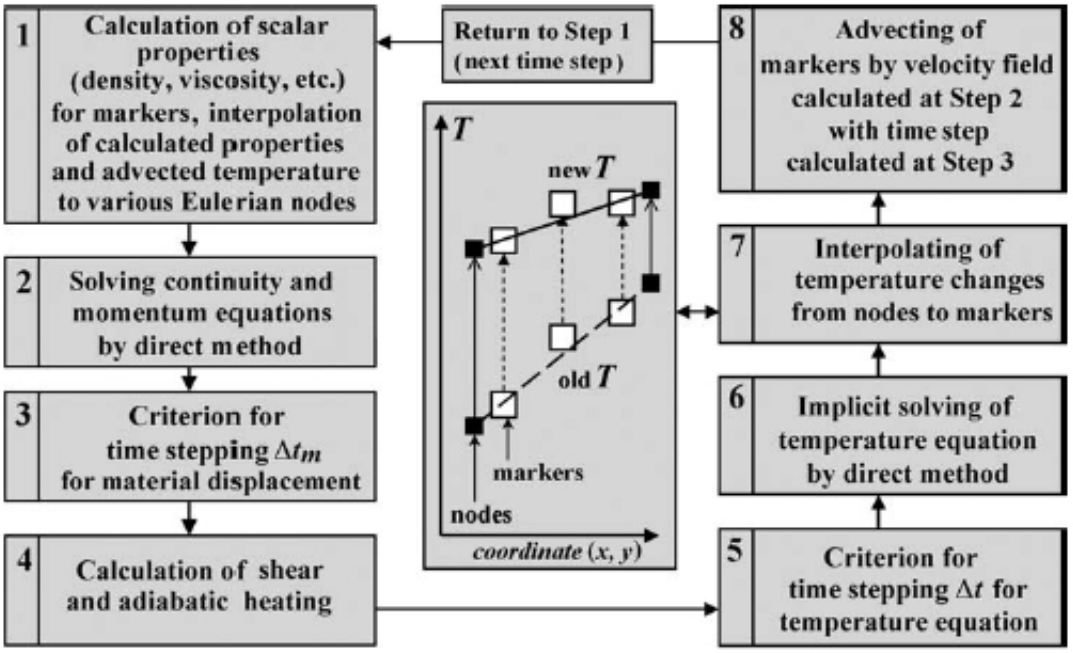

Fig. 2.5: Flow chart representing all the numerical step of I2VIS. The central panel is a graphical representation of the numerical techinque used for the temperature field [Gerya, 2009].

synthetic representation of the numerical step).

1. All the scalar properties prescribed on the markers as a function of the environmental variables (pressure and temperature), and the stress and strain rate fields [11]. Then, all the scalar properties as well as the temperature field of the advected marker are interpolated to Eulerian grid node.

2. 2D Continuity and Stokes equations are solved together in the Eulerian grid, in order to obtain the velocity and pressure field. From the velocity field is possible to calculate the deviatoric stress tensor and the deviatoric strain rate tensor components.

3. An optimal displacement time step for the marker is calculated Δt_m, following

[11] η depends on the P-T conditions and on the second invariant of either stress or strain rate tensor see section 2.2.2.

the Courant's condition[12].

4. H_s and H_a are calculated in the Eulerian grid nodes.

5. An optimal time step for the temperature equation is calculated.

6. Heat Balance equation is calculated in the implicit Lagrangian formulation.

7. Interpolation of ΔT from the nodes to the marker.

8. All the marker are displaced through the Eulerian mesh with fourth order Runge Kutta scheme. After the displacement, I2VIS returns to the step 1.

[12]Courant−Friedrichs−Lewy condition:it is a necessary condition for the convergence of a particular class of PDE, usually the hyperbolic ones, that are solved numerically with the finite difference method.

Symbols	**Meaning**
A_D	Pre−exponential factor material constant $MPa^{-n}s^{-1}$
C_p	Isobaric heat capacity (JK^{-1})
c	Cohesion (Pa)
E_{att}	Activaction Energy $(KJmol^{-1})$
g	gravitational acceleration (ms^{-2})
H_r,H_a,H_s,H_l	Radiogenic, Adiabatic,Viscous shear, Latent Heat (Wm^{-3})
k	Thermal Conductivity $(KJmol^{-1})$
M	Volumetric degree of melt
n	Stress exponent
P	Dynamic Pressure (Pa)
P_f	Fluid Pressure (Pa)
P_l	Lithostatic Pressure (Pa)
q_x,q_z	Heat flux (Wm^{-2})
R	Gas Costant $J\ mol^{-1}K^{-1})$
t	Time (s^{-1})
T	Temperature *(K or °C)*
v_x,v_z	Velocity $ms^{-1})$
V_{att}	Activaction Volume $(J\ MPa^{-1}mol^{-1}\ )$
α	Thermal expansion coefficient (K^{-1})
η	Viscosity $(Pa\ s^{-1})$
λ	Pore fluid factors
ρ	Material density $(Kg\ m^{-3})$
$\epsilon_{i,j}$	Strain tensor
$\dot{\epsilon}_{i,j}$	Strain rate tensor (s^{-1})
$\dot{\epsilon}'_{i,j}$	Deviaotoric strain rate tensor (s^{-1})
$\dot{\epsilon}'_{II}$	Second invariant of the deviaotoric strain rate tensor (s^{-1})
ϕ_{dry}	Dry frictional angle
$\sigma_{i,j}$	Total stress tensor $(Pa))$
$\sigma'_{i,j}$	Deviatoric stress tensor (Pa)
σ'_{II}	Second invariant of the stress deviatoric tensor (Pa)

Tab. 2.3: Symbol and unit

Chapter 3

Results

3.1 Numerical Setup

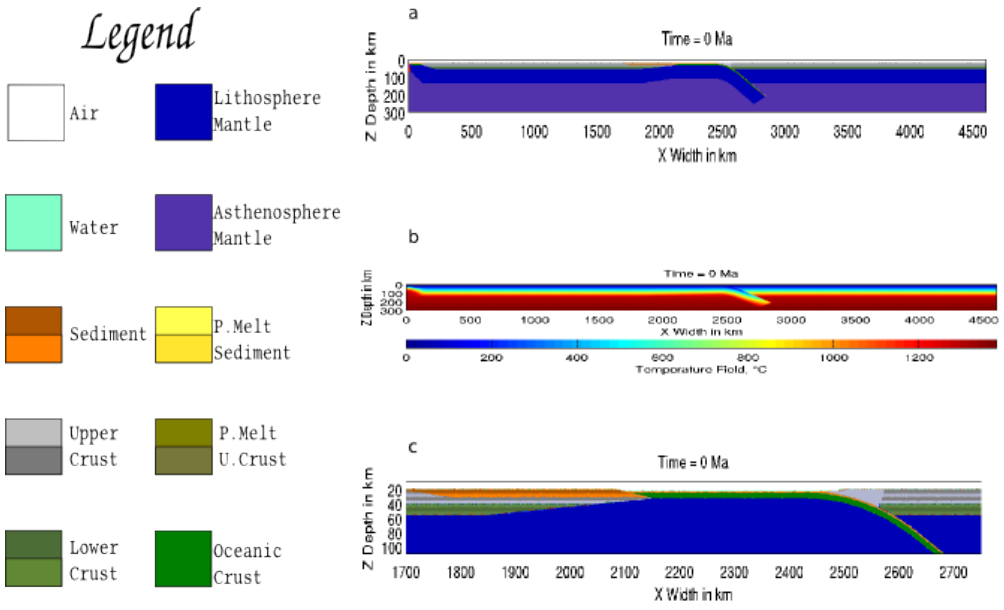

Fig. 3.1: Initial setup: left, the legend of the rock type used;a)Initial geometry;b)Initial thermal structure;c)Zoom of the initial geometry in the zone of interest

The numerical initial setup is designed for the study of post-subduction continental collision [Faccenda et al., 2008]. The *4600x300 km* numerical domain is irregular spaced and characterised by *509x101* Eulerian nodes. The grid spacing spans from *30 km* to *2 km* along x, and from *4 km* to *2 km* along z direction. The high resolution area with *2 km* spacing in both direction, spans from *2060 km* to *2750 km* along x, and from *0-100 km* along z. 2.1 milions of marker are used in the

simulation (see Fig.3.1).

3.1.1 Initial Geometry and Geotherm

The initial geometry of the model is the following: two continental plates (left plate and right plate) are separated by an oceanic plate which is bended below the right in order to simulate a spontaneous subduction process. The lower and upper crust of both the continental plates have the same physical properties, in order to distinguish the two crustal sequence i'll use the following acronyms:

1. L.U.C. (left upper crust) and L.L.C (left lower crust) for the crustal material of the left plate;

2. R.U.C (right upper crust) and R.L.C.(right lower crust) for the crustal material of the right plate.

The vertical sequence is: crust,lithospheric mantle and asthenospheric mantle. Crustal units have variable thickness: the continental crust thickness is *36 km* in both the continental plates and it is composed by *15 km* of lower crust and by *21 km* of upper crust; the oceanic crust thickness is *6 km*. The lithospheric mantle thickness is determined by the imposed thermal structure.

The passive margin at the transition of the left continental plate and the oceanic basin is characterised by the presence of *10 km* thick and *200 km* wide sedimentary sequence, reflecting the discharge of the continental interiors. The left margin of the right plate is characterised by an initial crustal orogenic wedge formed by the incipient subduction. All the rheological properties of the rock are listed in Tab.3.1

I shortly introduce the importance of the high radiogenic value of the U.C. and passive margin sediments. As I mentioned in the introduction one of the principal aim of this thesis project is the reproduction of the first order feature of hot orogens with particular regards to the Himalayan range. The high temperature achieved by the Himalayan range can be reproduced by taking into account the high radiogenic productivity of the rocks. There are several consideration to do in regards to the high radiogenic heat production:

- the exhumed high grade metamorphic sequence has high radiogenic heat production $4 - 5 \mu W m^{-3}$ [Faccenda et al., 2008];

- the rock of the indian crust has highly and variable value of heat production [Kumar et al., 2009];

- the sedimentary sequence of the passive margin may be enriched of heavy mineral which contain radiogenic elements (eg. zircon) [Faccenda et al., 2008];

Consequently in order to reproduce the temperature field of hot orogens, the passive margin sediments have high radiogenic heat production value (5.0 $\mu W m^{-3}$).

As I mentioned in the chapter 2.2.4 in order to simulate the continental collision a fixed velocity is prescribed. This velocity is defined on the left plate at x=1500 km and it is $2.5 cmyrs^{-1}$ for all the simulations. This is the velocity at which the Indian Plate subduct with the respect to the overlying Tibet. During the early stage of the simulation the oceanic plate subduct underneath the right plate. After the subduction of the oceanic plate, the collisional collision takes place.

The geotherm used for all the simulations is parametrised with the depth. The geotherm is calculated by using a linear interpolation between fixed temperature values at specific depths:

- $0°C$ at $z = 19km$ (and for all air and water particles);

- $249°C$ at $z = 33km$;

- $400°C$ at $z = 55km$;

- $1300°C$ at $z = 140km$;

I used a cold geotherm in order to reproduce the strength of the Indian Crust [Burov et al., 2014]. The temperature at the Moho is a key parameter because the crustal rock strength is highly dependent on temperature [Burov et al., 2014]. If the temperature of the Moho is high, the continental crust is weak and therefore it may accommodate the shortening induced by the convergence with pure shear thickening and folding. These two deformational processes may inhibit the burial processes [Burov et al., 2014].

Rock Composition	Flow Law	A_D	E_{att}	V_{att}	n	τ_{trans}	(1-λ)	c	$sin(\phi_{dry})$	ρ_0	H_r
Sediment	Wet Quarzite	$1.97{\cdot}10^{17}$	$1.54{\cdot}10^5$	0.8	2.3	$3{\cdot}10^7$	0.6	10^6	0.1	2600	$5{\cdot}10^{-6}$
Upper Crust	Wet Quarzite	$1.97{\cdot}10^{17}$	$1.54{\cdot}10^5$	1.2	2.3	$3{\cdot}10^7$	1	10^6	0.4	2800	$2{\cdot}10^{-6}$
Lower Crust	Mafic Granulite	$1.13{\cdot}10^{21}$	$4.45{\cdot}10^5$	0.8	4.2	$3{\cdot}10^4$	1	10^6	0.4	3000	$0.25{\cdot}10^{-6}$
Oceanic Crust	Mafic Granulite	$4.8{\cdot}10^{22}$	$2.38{\cdot}10^5$	0.8	3.2	$3{\cdot}10^7$	1	10^6	0.15	3000	$0.25{\cdot}10^{-6}$
Mantle	Dry Olivine	$3.98{\cdot}10^{16}$	$25.32{\cdot}10^5$	0.8	3.5	$3{\cdot}10^4$	1	10^6	0.6	3300	$2.2{\cdot}10^{-8}$

Tab. 3.1: Table of the rheological properties of the materials.The flow law are modified in order to increase the strength of the crust. This values are used for TestB4

Standard Transport equation values	
z_{eros}	20000 m
v_e	$0.3156\left(\frac{mm}{yrs}\right)$
κ_e	$0\left(\frac{1}{yrs}\right)$
κ_{mon}	0
t_{mon}	...
s_{sed}	$20500m$
v_s	$0.03156\left(\frac{mm}{yrs}\right)$
κ_S	$0\left(\frac{1}{yrs}\right)$
ϑ_{max}	0.1

Tab. 3.2: Standard Transport equation values: These values are the set of parameters used in the simulation in which the focused erosion is not used.

3.1.2 $P-T-t$ path

In order to calculate the $P-T-t$ *path* is necessary to chose a particular set of Lagrangian particles. All the Lagrangian particles have a particular identification number, therefore, it is always possibile to follow all the history of the Lagrangian particles through the simulation. After the end of the simulation, a spatial interval is defined where the Lagrangian particles close to the surface (and, thus, virtually outcropping) are selected: for example, in $TestC3Mon_{c1}$ the space interval ranges from *2200 km* to *2400 km* along x and the Lagrangian particles are selected every *20 km*.

By using the *marker ID*, it then possible reconstruct all the P-T and rocktype of each of the selected marker that are registered in the output file.

The Lagrangian particles during the simulation may change rocktype, not only because they partially melt, but also because of erosional and sedimentation processes. The transport equation used to simulate the surface processes is not mass conservative: erosion transform the surface Lagrangian particles into air or water in order to simulate the erosion. The main shortcoming of using this equation is associated with the P-T-t paths. The interval selection of the Lagrangian particle must be chosen in order to avoid the accidental selection of the markers which were air or water through all the simulation: for example, if I chose the spatial interval near the trench the probability to pick a marker which does not have any relevant geologic information increases. In order to recreate realistic P-T-t path it is necessary to set the picking interval away from the sedimentary basin. The necessary condition to have reliable information about the metamorphic history is that the markers which are selected must have a burial and exhumational histories.

3.2 Symmetric Orogenetic style

3.2.1 General Feature

The symmetric models are characterised by the yielding of the right plate. During the initial stage of the simulation, the right plate is weakened by sub-lithospheric processes. During the subduction of the left plate the oceanic crust is heated enough to be partially melted: the batches of partially melted oceanic crust rises up and accumulate at the base of the right plate lithosphere. This process produces erosion of the right lithosphere which diminishes its mechanical properties. After the onset of the continental collision, the L.U.C. accumulated at lithospheric depth heats and part of it detaches from the subducting plate. After the detachment the hot material rises up to lower depth and wedge in between the R.L.C. and R.U.C.. The R.U.C. cannot bear the stress arising from the expansion of L.U.C. material: the L.U.C material is hot and transmits heat to the R.U.C. which is thermally weakened. The R.U.C. decouples from the lower crust, and is up-warped by L.U.C . The right plate crust is thickened, and due to the self-heating processes partial melting occurs. The partially melted zone is focused between the lower crust and the upper crust and migrates laterally. The L.U.C. continues to flow towards the right while flow towards the left is inhibited. The stress arised from the wedging of the L.U.C is high enough to yield the overriding plate which flexure downward. The variability of this models is low. The rheological parameter that I modified seems to be not influent on the development of this kind of models. I systematically varied the friction coefficient, activation volume, lambda factor. The only parameters that affects the simulation is the stress transition value. However the variation of this parameters leads to the emergence of asymmetric types of collisional zone which is described in the following section.

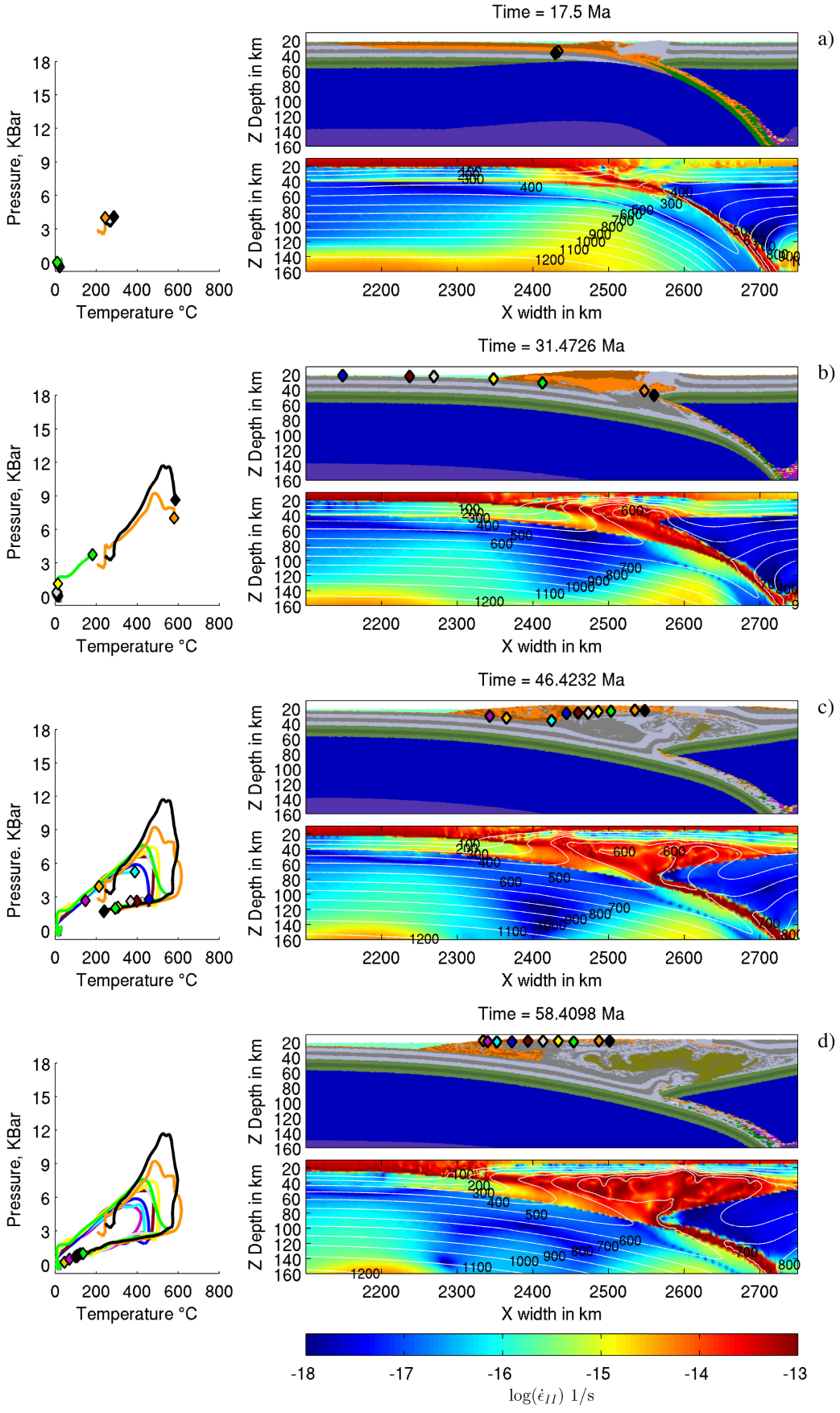
Time = 17.5 Ma
a)
Pressure, KBar
Temperature °C
Z Depth in km
X width in km
Time = 31.4726 Ma
b)
Time = 46.4232 Ma
c)
Time = 58.4098 Ma
d)
-18
-17
-16
-15
-14
-13
log($\dot{\epsilon}_{II}$) 1/s

Fig. 3.2: Each figure is composed by: P-T-t path (left); composition map (upper right),the selected Lagrangian Marker are plotted in the composition figure ; $log_{10}(\dot{\epsilon}'_{II})$ (under right) and isotherms (whitelines); This panel represents the time evolution of the reference TestB4.

3.2.2 Reference Model

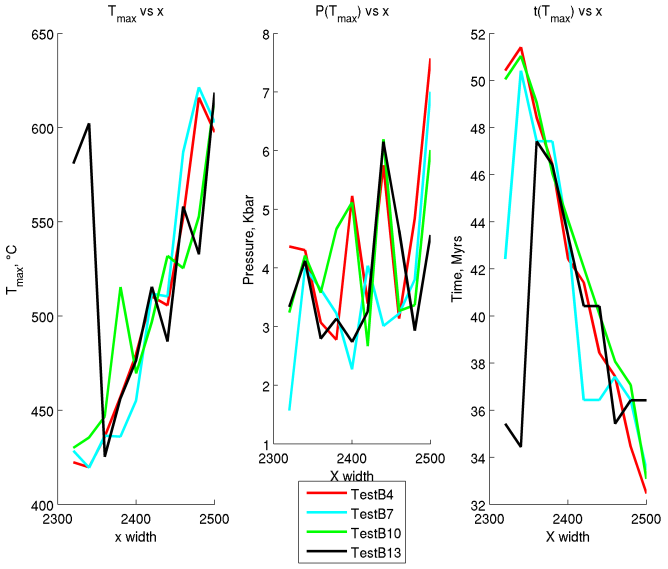

Fig. 3.3: **Left**:The maximum temperature against the x position of the Lagrangian markers is plotted. T_{max} increases toward the centre of the orogenic system;**Center**:The pressure at which the lagrangian particles achieved T_{max} is plotted, the pattern is more chaotic; **Right**:The time of achievement the maximum temperature against the x position, the timing of the metamorphic peak diminishes toward the center of the orogenetic system.

I choose as reference model TestB4.(see Tab.3.1)[1]. I shortly describe the evolution of this simulation:

- **0−17 Ma**(Fig.3.2a) The left plate converges according to the prescribed velocity. During the first 10 Myrs, the oceanic lithosphere is subducted. The sediments lying above the oceanic crust, are mostly subducted in the subduction channel. Soon after the total consumption of the oceanic crust of the left plate, the accretionary prism is uplifted and the R.U.C is up-warped. Since the

[1]In this kind of test, I did not use the focused erosion. All the transport equation values are listed in Tab.3.2

rheological coupling between the R.U.C and R.L.C. is weak, the two crustal units do not deform together: all the strain is accommodated by the R.U.C.;

- **17−31 Ma**(Fig.3.2a-b): During this time interval the highly radiogenic passive margin sedimentary unit approaches the accretionary prism. The interface between the L.U.C. and the passive margin sedimentary unit becomes a décolement surface: the L.U.C is under-thrusted below this surface, while the sediments are accreted at the surface. Soon after the dcolement surface is formed, the L.U.C. deforms and part of it starts to rise up or to be transported leftward together with the passive margin sedimentary cover. During this time interval, the R.U.C. and R.L.C. are totally decoupled and the L.U.C. starts to wedge between the R.L.C and the R.U.C. . The right plate starts to yields.

- **31−46 Ma**(Fig.3.2b-c): The L.U.C. continues to be transported towards the right being accumulated between the R.U.C. and R.L.C. . The rapid accumulation of L.U.C. material in the right plate produces a localised load which causes the downward flexure of the right plate. L.U.C. material on the right plate is partially melted .

- **46−58 Ma** (Fig.3.2c-d): After the production of p.m.U.C., the flow field starts to be chaotic. The shape of the partially melted region is irregular and progressively expands leftwards. This produce a reactivation of the décolement surface on the left. The L.U.C material, which is forced to flow leftward, starts to partially melt, and batches of melt are produced at the center of the orogenic belt.

In the initial stage of the simulation the uplift focuses around the trench. As soon as the right plate starts to yield, the R.U.C. starts to be uplifted. The uplift of the right side propagates together with the deep flux of L.U.C. material between the R.U.C. and R.L.C. The results is a wide orogenic plateu. During the on-set of the continental collision the orogen achieves the maximum elevation, which is gradually smoothed by erosion as soon as the right plate starts to yield. Even if the region does not experience to uplift, the surface continues to be highly corrugated. The

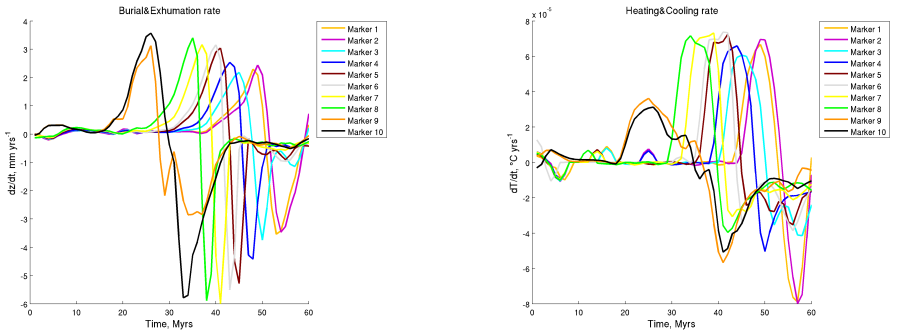

(a) (b)

Fig. 3.4: a)Burial and Exhumation rate: the positive values indicate burial processes, while negative values indicate exhumation processes; b) Heating and cooling rate, positive values indicate heating processes, negative values indicates cooling processes. The Burial processes are consecutive, the peack velocity is achieved in different time for each selected Lagrangian particles. The heating processes start during the burial processes and continue during part of the exhumation path. During the exhumation the L.Markers are heated, then they are cooled at costant rate.

corrugation augments in the last stage of the simulation, these corrugations are associated with extension of the uppermost part of the orogens due to the development of a dome-like structure (at 2600 km)(Fig. 3.6).

The maximum temperature achieved by the U.C is 650 °C. The high temperature zone closely follows the shape of the partially melted region (see Fig. 3.5).

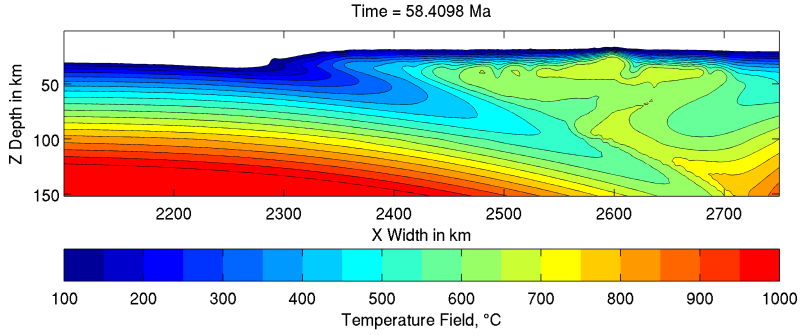

Fig. 3.5: Countur of the temperature field at last time step of TestB4.

The Lagrangian particles followed during all the simulation are selected between 2300−2500 km. The maximum temperatures achieved by the markers augment toward the right. The temperatures achieved spans from $419°C$ to $615°C$. Even if the maximum temperature shows a trend, the pressure achieved by the markers in the T_{max} does not show any specific trend (see Fig.3.3). On the other hand the absolute maximum pressure achieved by the markers augments toward the right as for the maximum temperature. The timing associated with the achievement of the maximum temperature decreases toward the right. Therefore the maximum temperature is achieved earlier toward the center of the orogenic belt. The markers are sequentially buried and exhumated (see Fig.3.4).

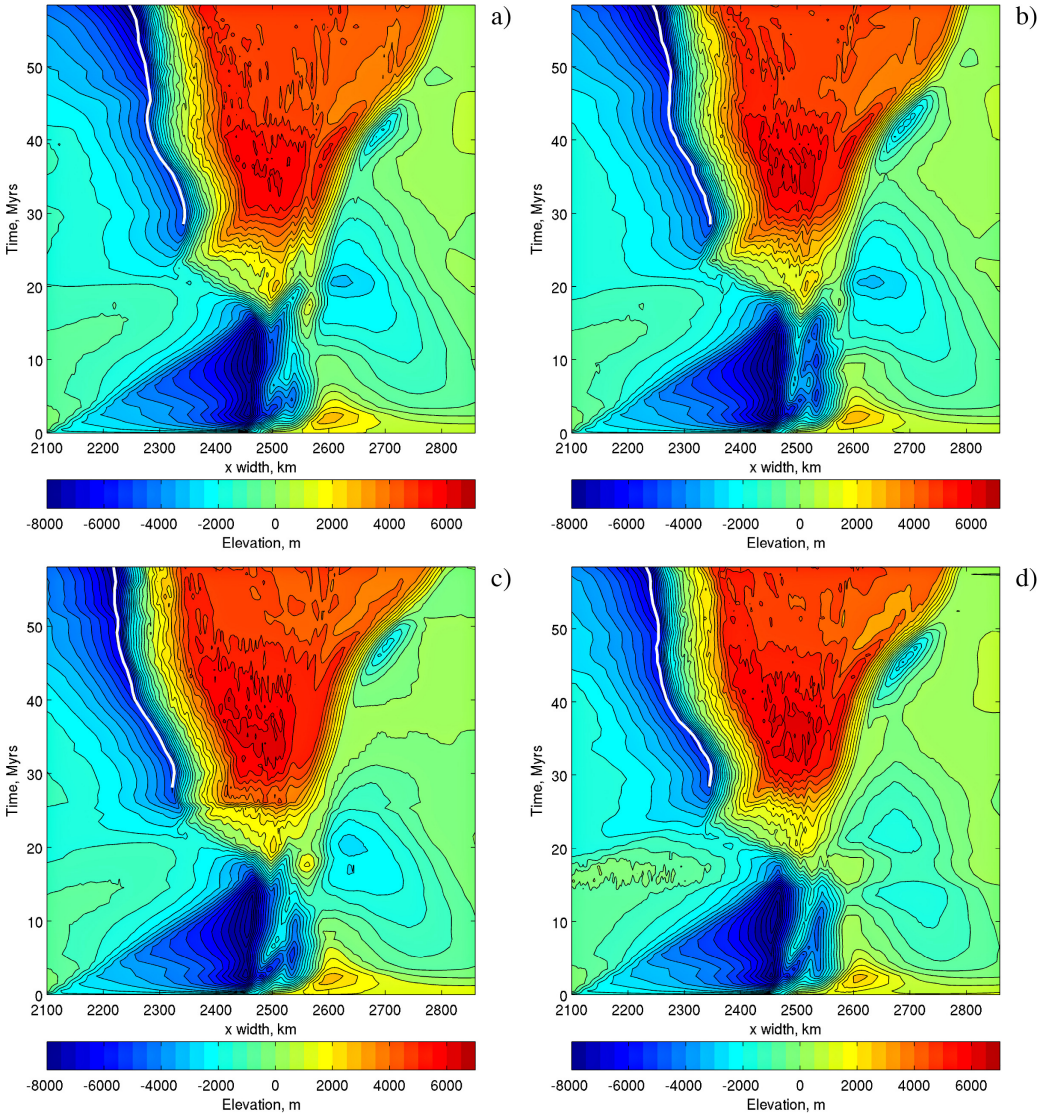

Fig. 3.6: Countour map of topography evolution in time.All the bidimensional profiles producted during the simulations are plotted togheter. The 2D profiles producted are exploited to interpolate and create the topography map.Each color represents interval of 500 m.In all figures the white line represents the position of the topography minimum. a) TestB4 topography evolution; b) TestB7 topography evolution; c) TestB10 topography evolution; d) TestB7 topography evolution.

3.2.3 Examination of the effect of the friction angle

Test	Rock Type	$sin(\phi_{dry})$
TestB7	Upper Crust	0.5
TestB10	Upper Crust	0.6
TestB13	Upper Crust	0.4−0.2

Tab. 3.3: Parameters modified in respect to the reference TestB4

In this kind of model I have not modified the surface processes parameters. Conversely, I systematically varied the plastic rheological parameter. Despite the numerous parameter varied, the variability of this kind test is low, all the first order feature of the simulation is preserved. I shortly introduce three test: TestB7, TestB10 and TestB13 (see Tab3.3), in which I have changed the friction coefficient of U.C. .

The evolution is quite the same for all the model except for the TestB10. High value of the frictional coefficient delay the wedging of the L.U.C. between the R.U.C and the R.U.C. . The delay of the wedging induce an initial propagation of the orogen toward the left: for example in TestB10 the partially melted region initially appears above the subducting plate. However, as soon as, the material is able to wedge between the R.U.C. and L.U.C., the simulation converges to the reference model results. Even the temperature field of this test at the end of the simulation is quite similar to the reference models. The topographic evolution is slightly different for each models. The retarded wedging of the L.U.C between the R.U.C. and R.L.C. induces the material to flow toward the left; consequently, the topography evolves above the left plate. As soon as the R.U.C. yields the uplift rapidly focuses on the right plate. (see Fig. 3.6). The metamorphic grade augments toward the right, while the t(T_{max}) diminishes in the same direction. The cooling rate indicates that

the Lagrangian particles are sequentially buried and exhumed in all this kind of model. As for the reference model the maximum pressure achieved by the Lagrangian particles increases towards the right. In all these test Lagrangian particles do not melt(see Fig. 3.3).

Despite the presence of little differences between these simulation, the main feature of the reference test is preserved. I performed other models in which I have modified other parameters, and the results are similar to the reference models. The secondary effects of the rheological parameters modified during all the simulation are associated with the timing of right plate yielding and the occurrence of partial melting. If a strong plastic rheology is used, the wedging of L.U.C. material between the R.U.C. and the R.L.C. is retarded, which may produce both the production of melt above the left plate and an initial development of the orogen towards the left side.

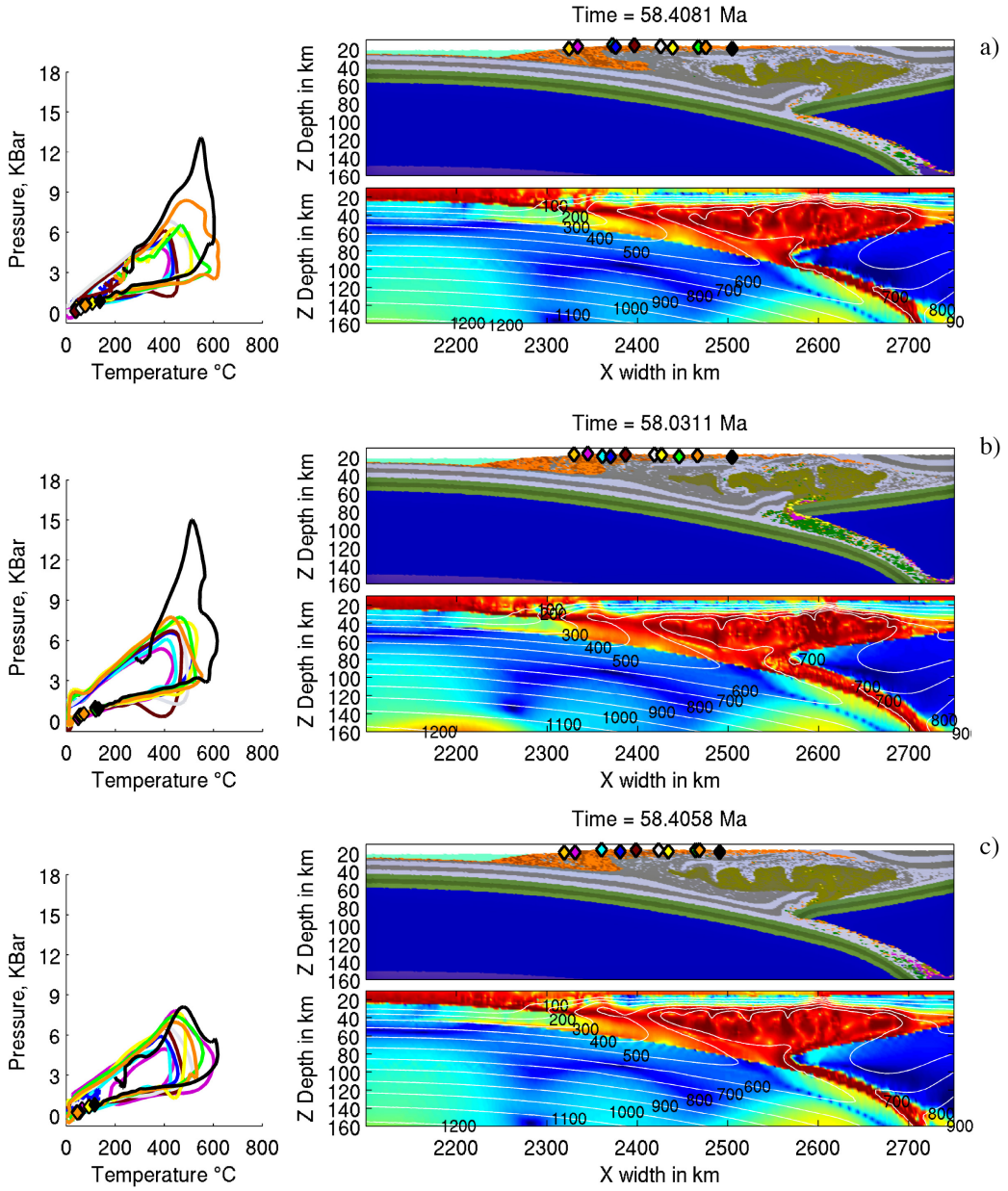

Fig. 3.7: Comparison of the last time step of: a)TestB7; b) TestB10; c) TestB13

3.3 Asymmetric Orogenetic style

3.3.1 General Feature

	U.C. $sin(\phi_{dry})$	U.C. V_{att}	L.C. $sin(\phi_{dry})$	L.C. V_{att}	M.L. V_{att}	U.C. H_r	τ_{trans}
TestC3	0.4	1.0	0.6	1.0	0.8	2.5	$3\ 10^4$
TestC3'	=	=	=	=	1.0	2.0	=

Tab. 3.4: TestC3 parameters. TestC3' is the modified Test.

In this kind of model, the upper crust of the right plate is coupled with the lower crust, and it is able to bear the compressional stress without deforming.The strength of the U.C. is determined by the value of τ_{trans} (see Tab. 3.4). All the model are characterised by a fixed value of stress transition ($3 \cdot 10^4$ MPa).Because of the high strength of the upper crust the material which comes from high depth is not able to wedge between R.U.C. and R.L.C. as in the symmetric model. So, for this reason, there is no mass transport to the right plate, and all the material, which was deeply accumulated during the continental collision, is advected toward the foreland above the left plate for all the duration of the collision . Consequently, there is a rapid evolution of the topography on the left side of the collision zone, and a propagation of the compressional front in the same direction. The material flux can be seen as a megascopic corner flow. The accumulation of L.U.C. at lithospheric depth produce a deeply buried zone, in which the acid rocks are heated. Since the heating processes decreases the viscosity, part of L.U.C. material decouples from L.L.C. which continues to be subducted. After the decoupling the L.U.C. rocks start to upwell and eventually partial melting occurs. More in detail L.U.C can be divided in two main portions: the lowermost U.C. is underthrusted [2] below the upper plate and, thus, it is transported toward the right, while the uppermost U.C. is involved in the return flow and flow toward the left; the latter one can be divided in two zones in respect to the rheological behaviour: the uppermost part is rigid, cold and shows brittle behaviour, the lower one is hot and show viscous behaviour. The u.U.C. can be either rigid or ductile, with the rheological behaviour depending on temperature. The strength of the u.U.C. is important for the dynamic of the overlying hot and partially molten crust [3]. If the u.U.C. maintains its strength

[2] u.U.C. is the acronomy that will be used to distinguish the two portion
[3] p.m.U.C. is the acronomy for the partially molten crust

during the burial processes, the p.m.U.C. is forced to advect between the uppermost brittle layer and it, on the other hand, if the u.U.C. is weakened the p.m.U.C. starts to tunnel it. I extensively used this kind of result to perform numerous test in which I systematically varied all the surface processes parameters. The aim of these tests is to verify if surface processes can influence the evolution of the orogen and if the p.m.U.C. flow can be influenced by an highly focused erosion acting on the left flank. I tried to use a standard set of surface processes parameters in order to compare all the tests. One of the most important parameters influencing the model results is the sedimentation rate, which provides weak and highly radiogenic material to the propagating left front of the orogenic belt.

3.3.2 Reference Model

The reference model that I chose for this kind of test, is TestC3. All the parameters that were used are listed in table 3.4. This test was the starting point of a set of models in which I implemented focused erosion, in order to simulate the Himalayan tectonic evolution and monsoonal style of erosion. The major shortcoming of this model is the high radiogenic heat production. In spite of its being a perfect paragon for this kind of model, TestC3 is too sensitive to sedimentation parameters: if the sedimentation input is augmented, the high radiogenic sediments heat the L.U.C., which is then weakened enough to:

- undergo a pure-shear deformation (pure-shear thickening and pure-shear folding)
- initialise the tunneling mode propagation of the partially melted crust.

In order to investigate realistic sedimentation rate and erosion rate parameters in the simulation in which is implemented the focus erosion, H_r is diminished from 2.5 to 2.0 $\mu W m^{-3}$.

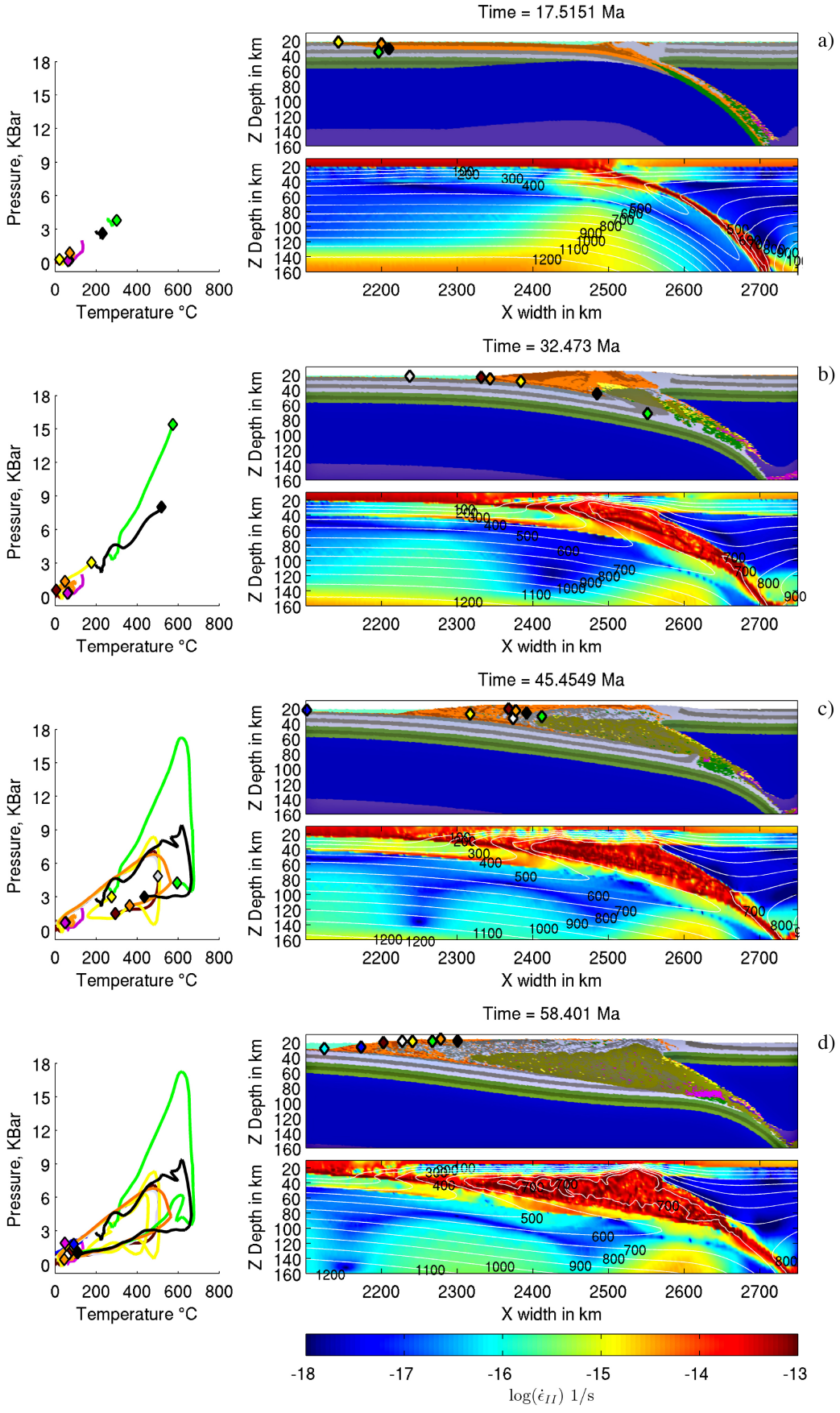

Fig. 3.8: TestC3 evolution

Temporal Evolution

- **0-17 Ma**(see Fig. 3.8.a):As for the other models, in the first ten million years the left plate converges towards the right plate according to the imposed convergence velocity. During this time interval, the initial accretionary prism is deformed and down-warped. The initial topographic response is the creation of a sedimentary basin on the trench outer-rise. During the oceanic crust subduction, the left plate dip angle changes and this produces an injection of the previously subducted buoyant material on the subduction interface. The subduction channel material is a complex mélange composed of slices of oceanic crust, sediments and continental crust. During the initial stage of continental collision, highly radiogenic sediments of the passive margin are accreted to the accretionary prism, which is then up-warped and undergoes a rapid uplift.

- **17-32 Ma**(see Fig. 3.8.a-b): The sub−lithospheric material starts to interact with the deeply transported L.U.C material, which is heated enough to detach from the lower crust and to riseup. Soon after the detachment from the lower crust, L.U.C. starts to melt. The partially melted crust migrates toward the pro-foreland, since the right plate upper crust is able to bear the stress which arises from the collision. The material flux describes a corner flow like trajectory, mass transport is accommodated by a décollement surface, which intersects the surface at the thrust front.

- **32-45 Ma**(see Fig. 3.8.c):The p.m.U.C. is channelled between the upper brittle layer and the strong u.U.C.. The shape of the partially melted region is triangular.

- **45-58 Ma** (Fig. 3.8.c-d):In the final stage of the model, near the suture zone, a dome-like structure develops

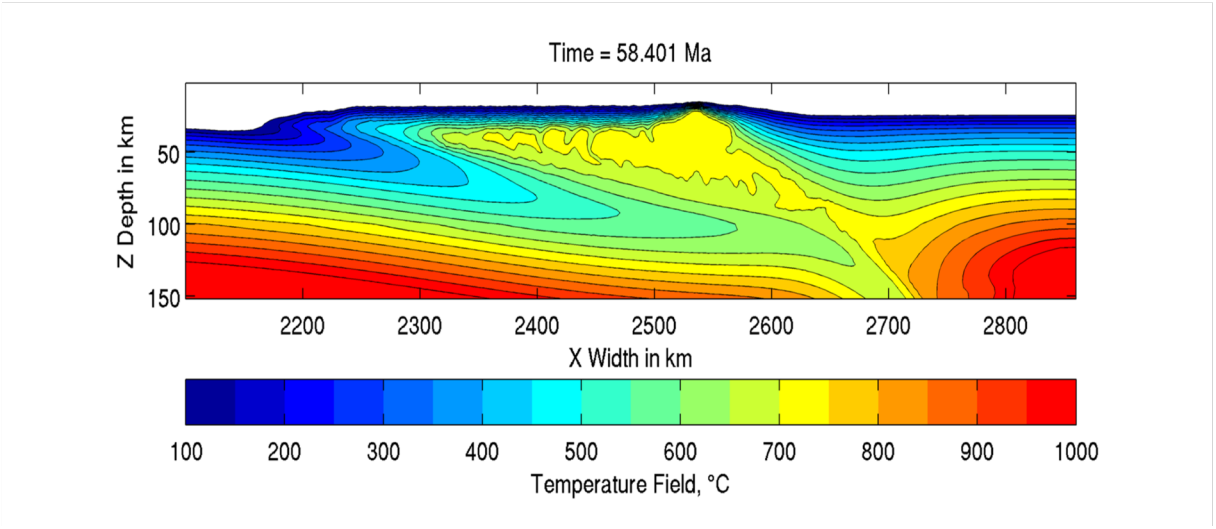

Fig. 3.9: Countour of the temperature field of TestC3 at the end of the simulation

The p.m.U.C. is voluminous and the temperatures in the core of the orogen are high (700 °C, see Fig. 3.9). The high temperatures and the partially melted crust are the result of the radiogenic heating processes, which are enhanced by the high H_r value (H_r =2.5 $\mu W m^{-3}$) of the Upper Crust. I performed several tests in which I varied the H_r production of the U.C.. The necessary condition for the emergence of the asymmetric orogenetic styles is the strength of the U.C., consequently the H_r plays an important role in the development of this kind of orogenetic styles. The critical value of H_r is 2.5 $\mu W m^{-3}$. If the H_r value is higher than the critical value the simulation starts to converge to the symmetric orogenetic style. TestC3 is the best example of the asymmetric models, but it has several limits due to the high radiogenic heat production of the U.C. The sedimentation rate cannot be increased, because the u.U.C, starts to buckle even for a little increasing of v_e.On the other hand, the tests with low radiogenic heat production show a little difference with the reference test: the insertion of hot astenosphere material in the subduction channel. This sub−lithospheric processes does not happen if the sedimentation rate is increased from the basic sedimentation rate (see Tab. 3.2). I used TestC3 as a reference because it is representative of this kind of simulation, but it is necessary to highlight that there is a complex interplay between rheology, radiogenic heat production and sedimentation rate. The insertion of the asthenospheric material is not a intrinsic feature of the asymmetric models, it probably emerges because, for the tests TestC3', I changed the activation volume of mantle lithosphere (from 0.8 to

1.0 $JMPa^{-1}mol^{-1}$). This issue is intriguing, but it is far from the aim of the thesis project, consequently I prefered to use the tests in which I had tested all the surface processes that I had created, in order to investigate the interplay between partially melted crust and the surface processes. However, the interplay between the several altered parameters does not change that: the necessary condition for the emergence of the asymmetric orogenetic style is the crustal strength, and the critical value for the transition between asymmetric and symmetric orogenetic style is τ_{trans}. I choose this test as reference for the evolution of the asymmetric models, because it is the base for the test in which I implemented the focused erosion and because it shows that the focused erosion is not necessary for the exhumation of the partially melted rocks and for the low viscosity channel.

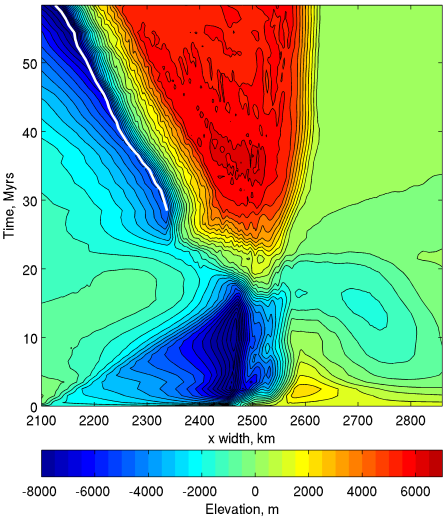

Fig. 3.10: TestC3 topography evolution

The topographic response is illustrated in the Fig. 3.10 . After the collision, a narrow belt starts to uplift. The first important feature is the migration of the trench toward the left. The collision zone can be divided into two main zones, the left flank and the plateu. The first is characterised by a steep topographic gradient, the latter is characterised by a more gentle slope.

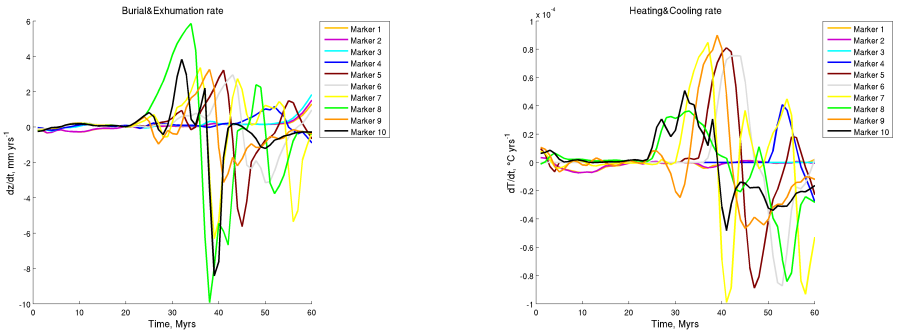

(a) (b)

Fig. 3.11: a)Burial and Exhumation rate: the burial process is positive, while the exhumation process is negative. The exhumation rate is asymmetric: as soon as the exhumation starts, the velocity is high, after the achievement of the maximum rate, the velocity diminishes with a different slope ; b) Heating and cooling rate: heating rate is positive, cooling is negative. As for the exhumation stage, there is an asymmetry in the cooling rate. The change of the slope corresponds to the quasi-isobaric cooling.

As shown in the evolution of the orogen, after the initial stage of continental collision, the selected markers start to be buried. Later, when they reach the core of the orogen, they begin to rise up and eventually to melt. Markers are advected in the hot, partially melted channel. After they reach the tip of the hot channel, they begin to solidify: the cooling processes at the end of this stage is quasi-isobaric. As shown in Fig. 3.11, the burial and exhumation processes start sequentially, and quasi-isobaric cooling occurs for almost all the markers at the end of the run.

3.3.3 Surface Modelling

The asymmetric models are chosen to investigate the complex interaction between tectonic processes and surface processes. Several studies have been done in order to investigate if there exists any positive or negative feedback between tectonic and surface processes [Burov and Toussaint, 2007, Toussaint et al., 2004, Chen et al., 2013]. In one of the most important exhumational model for the Great Himalayan sequence, focused erosion plays a fundamental role: it is the necessary condition for the exhumation of GHS [Beaumont et al., 2001, Beaumont et al., 2004].

In order to reproduce all the first order characteristics of the Himalayan range, I calibrate the erosional parameters following different values from the literature. The erosional patterns are complex, with erosion rates varying both across the range and

along its strike [Thiede and Ehlers, 2013]. Despite the complexity of the erosional rate pattern, for evaluating the first order implication of the erosion, I chose to use an simplified elevation dependent, focused erosion, which starts at t_{mon}. The timing of the initialisation of the erosion is one of the most controversial, I used as reference t_{mon} *38 Ma* after the model initialisation. The starting point is the reference model TestC3, which was modified in order to use different values of sedimentation. In the simulations in which the monsoonal erosion is implemented, H_r value is lowered(see Tab. 3.4): this implies less radiogenic heat production and thus, lower temperatures. For the surface processes I used a standard set of parameter Mon_{c1} (see Tab. 3.5 for erosion parameters).

Parameters	Mon_{c1}	Mon_{c1s1}	Mon_{c1s2}	Mon_{c1s3}	Mon_{c1}^{45Ma}	Mon_{c1}^{50Ma}
z_{eros}	20000 m	=	=	=	=	=
v_e	0.3156 $\left(\frac{mm}{yrs}\right)$	=	=	=	=	=
κ_e	1.57 10^{-4} $\left(\frac{1}{yrs}\right)$	=	=	=	=	=
κ_{mon}	4	=	=	=	=	=
t_{mon}	38 Ma	=	=	=	45 Ma	50 Ma
s_{sed}	$20500m$	=	=	=	=	=
v_s	$0.1578\left(\frac{mm}{yrs}\right)$	0.0789	0.2367	0.3156	0.1578	=
κ_S	0 $\left(\frac{1}{yrs}\right)$	=	=	=	=	=
ϑ_{max}	0.3	=	=	=	=	=

Tab. 3.5: Surface processes parameters.These are the standard set of surface parameters. Each standard set is applied to TestC3'.

TestC3'Mon$_{c1}$ and sedimentation parameters

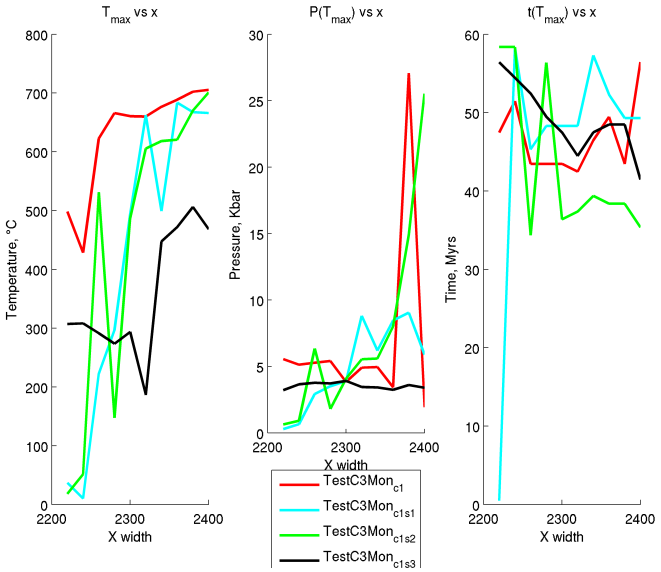

Fig. 3.12: Left: T$_{max}$ against x. In all test performed the temperature increases with the structural level. The increasing of temperature with the structural level has a general trend. Centre: Pressure at T$_{max}$: The pressure at the max temperature against x, is not clear except for TestC3Mon'$_{c1s2}$ and TestC3'Mon$_{c1s3}$, in which P(T$_{max}$) increases with the structural level. Right: in all performed test t(T$_{max}$) does not have any general trend.

TestC3Mon'$_{c1}$ is used as a reference model for the simulation of surface processes. The sedimentation rate (v_s) has been varied from 0.0789 to 0.3156 mmyrs^{-1} . Since the sediments have a weak rheology and high radiogenic heat production, the variation of v_e exerts an important role in the evolution of the orogen. The induced deviations from the reference model are not clear, and further studies must be done in order to calibrate these parameters. Firstly, if a low sedimentation rate is used, the leftwards migration of the décolement surface is inhibited, which can be linked to the unbalanced material flux with respect to the focused erosion which removes material. On the other hand, when a high value sedimentation rate is used, the evolution is controlled by the heating effect of the sediments rather than their weak rheology. In TestC3'Mon$_{c1s2}$, in which $v_e = 0.2367$ mmyrs^{-1}, the thrust propagation is efficient, but the underthrusted crust is weak enough to thicken(see Fig. 3.14.c).

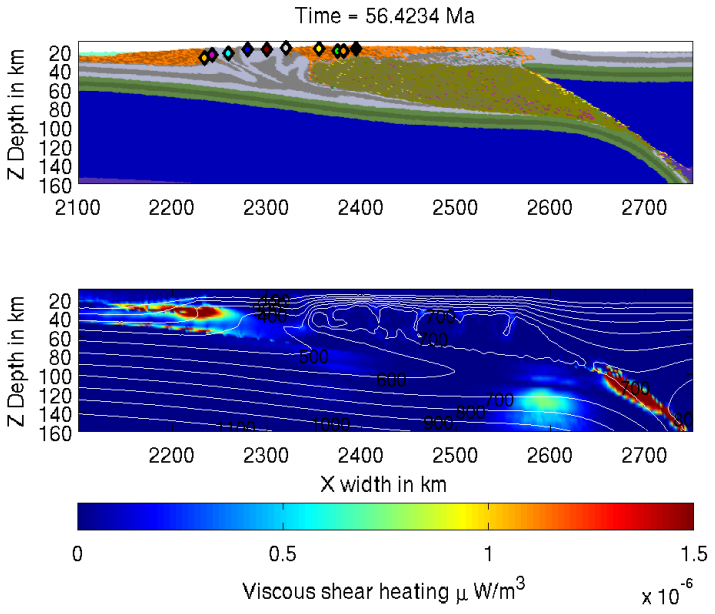

Fig. 3.13: This picture is representative of the transition from buckled crust to megathrust: The upper figure is the composition field, while the figure below is the viscous-heating production. The viscous heating is high in the narrow zone in which the megathrust is formed.

If higher values of sedimentation rate are used, the thick sedimentation cover heats the underthrusting crust which is weakened enough to buckle. The buckled crust stops the incoming material, which results in the formation of overthickened crust near the thrust front. The convergence still continues and the sedimentary basin formed in front of the buckled crust is highly strained. The deformation of the left sedimentary basin and of the U.C. buckled crust produces enough heat to localise the deformation along a low angle mega-thrust in the buckled crust. This behaviour had been described before by Burg [Burg and Schmalholz, 2008](see Fig. 3.13). The partially melted material starts to tunnel toward the left the newly accreted U.C.. After the initialisation of the crustal buckling, the main thrust surface dissolves in a wider high-strain rate zone. After the formation of the megathrust from the buckled crust, a new décolment surface arises on the contact between the u.U.C. and the foreland basin (see Fig. 3.14.d). The thermal effect of the sedimentation rate can be appreciated by looking at the isotherms at the thurst front. At lower temperatures the distance between two isotherms augments. The shape and the distance of the isotherms is usually function of the efficiency of the advective processes with respect to the conductive processes. The sigmoidal shape of the isotherms near the thrust front, in low v_e test, implies that underthrusted cold material maintains its

temperature even if passes through hot zone. The sediments are a weak material that lubricates the interface between the leftward thrust front and the rightward underthrusting processes. This effect is suppressed by increasing the sedimentation rate: a thick sedimentary cover produces enough heat to weak the u.U.C which viscously deforms. The temperature field is almost the same in all models, except for the test in which the highest sedimentation rate velocity is used: in this model two thermal zones can be distinguished, the interior one and the external one: the first is characterised by high temperatures (in the partially molten region of the model), the latter by low temperatures.

This zone is divided by the megathrust that forms during the evolution of the model(see Fig. 3.15).
All the lagrangian particles tracked during the simulation are picked between 2200-2400 km.From the P-T-t paths of the models presented here (except for the TestC3Mon$_{c1s3}$), it is possible to distinguish three stages:

- Rapid Burial: In this stage the markers are brought to high depth and they are heated;
- Rapid Exhumation: In which the markers are brought to low depth; this stage usually is quasi-adiabatic, the P/T gradient is low;
- Isobaric cooling: in which the markers cools at costant pressure.

TestC3Mon$_{c1s3}$ shows an anomalous behavior: two stages can be distinguished:

- Slow Burial: in which markers are heated;
- Slow Exhumation: in which markers cool and are brought to lower depth.

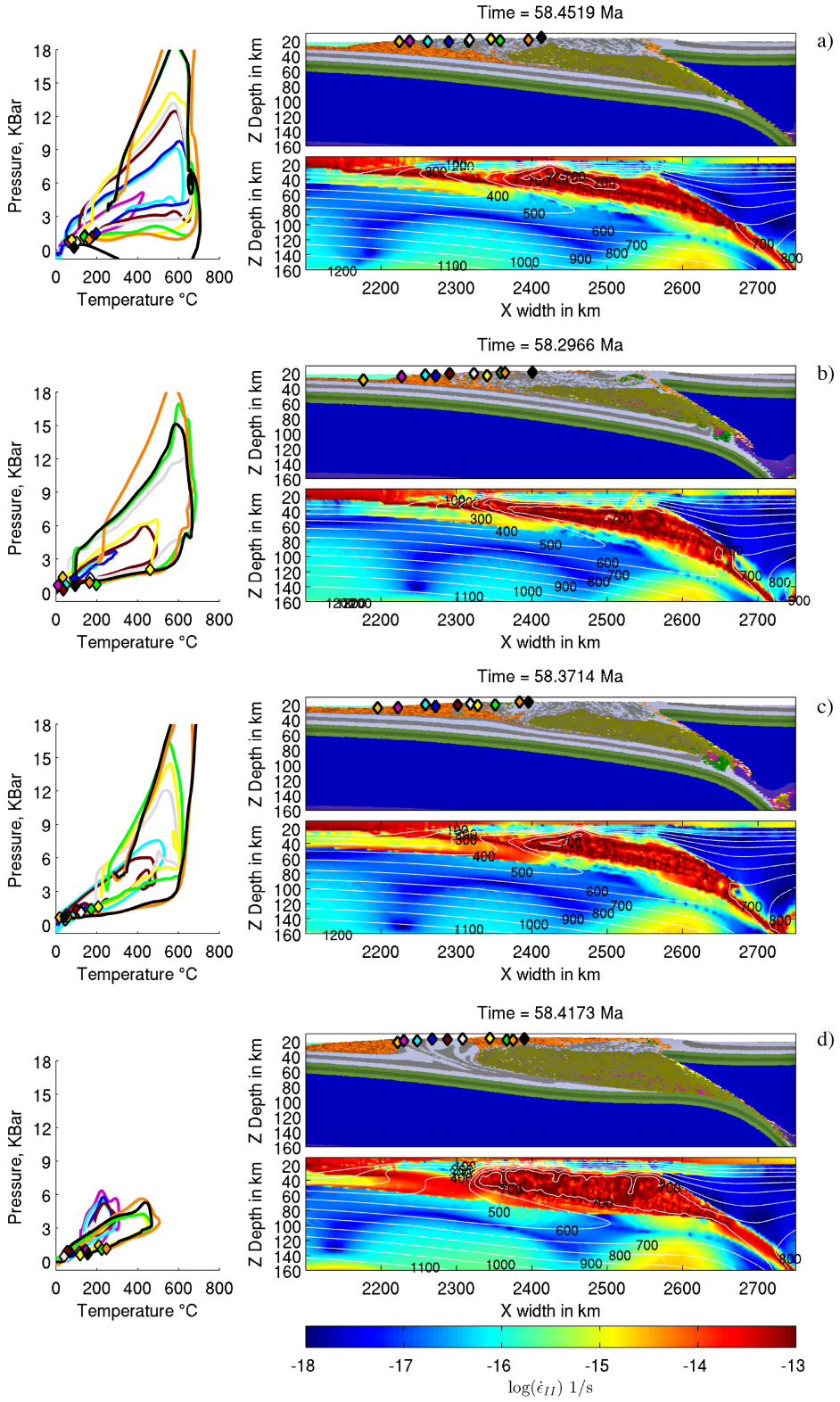

Fig. 3.14: Comparison between the sedimentation test: a) TestC3Mon'$_{c1}$; b) TestC3Mon'$_{c1s1}$; c) TestC3Mon'$_{c1s2}$; d) TestC3Mon'$_{c1s3}$

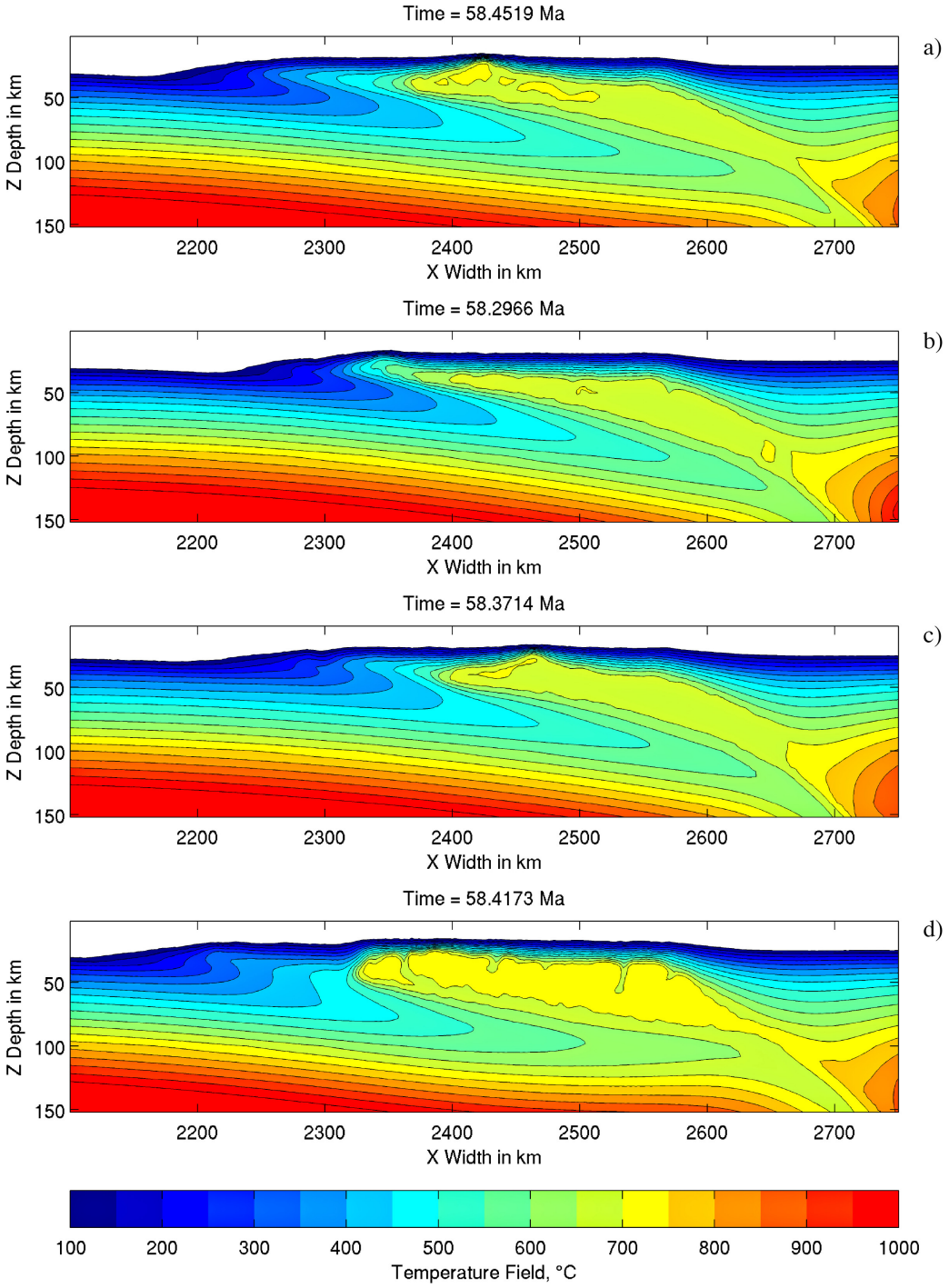

Fig. 3.15: Comparison between the last time step of the asymmetric test temperature field. a)TestC3Mon'$_{c1}$;b) TestC3Mon'$_{c1s1}$;c) TestC3Mon'$_{c1s2}$;d) TestC3Mon'$_{c1s3}$.

The reference model is characterised by an inverted metamorphic gradient: the markers temperature spans from 500 °C to 700 ° C. TestC3Mon'$_{c1s1}$ and TestC3Mon'$_{c1s2}$ have a similar behaviour, and the temperature is almost the same, except for the low structural markers which have lower temperatures because they have been picked close to the foreland basin sediment. P(T$_{max}$) is different for each test:

- TestC3Mon$_{c1}$ does not show any significative difference in all structural levels (except for the one (light orange, see Fig. 3.14a) which achieve UHP condition);
- TestC3Mon$_{c1s1}$ is complex, and show P(T$_{max}$) values which increase with the structural level, but in the uppermost markers show alternating low and high value(see Fig. 3.12).
- TestC3Mon$_{c1s2}$ shows a constant increasing of pressure with structural level. The t(T_{max}) does not show a strong correlation with the structural level(see Fig. 3.12).
- TestC3Mon'$_{c1s3}$ does not show any significant difference of P(T$_{max}$) value(see Fig. 3.12).

All the burial and exhumation processes are contemporaneous.

Topographic response is quite different for each test (see Fig. 3.16):

- TestC3Mon'$_{c1}$ The migration of the material is towards the left since the beginning of the simulation and the topographic evolution follow the migration of the compressional front.
- TestC3Mon'$_{c1s1}$: Since the migration processes are inhibited by erosionand the absence of a thick weak layer augments the frictional forces in the main decollement surface, the extension of the orogen is limited. One of the main difference in respect to the reference model is the corrugations in the plateu which continue to persist and do not decay with time; this is a direct consequence of the inhibition of the compressional front to the left (see Fig. 3.16 b).
- TestC3Mon'$_{c1s2}$: the compressional front migrate toward the left. In all the simulation the left sedimentary basin is not affected by the deformation, although in this test the foreland basin is affect by a pervasive deformation which

can be appreciate by observing the corrugation of the topography. The main difference is the geometry of the décolement surface (see Fig. 3.14.c). The main thrust surface is exposed at the trench through all the reference model TestC3, while in this test the main thrust surface split in two different branches and the compression pervasively affects the fore-land basin.

- TestC3Mon'$_{c1s3}$: The topographic evolution is complicated, the generation of the megathrust induces first order modification of all the dynamics. This induce a completely different topographic response. The compressional front migrates toward the left as in other simulation, but compression is still maintained in the interior of the orogen, which produces a highly corrugated surface (see Fig. 3.16 d).

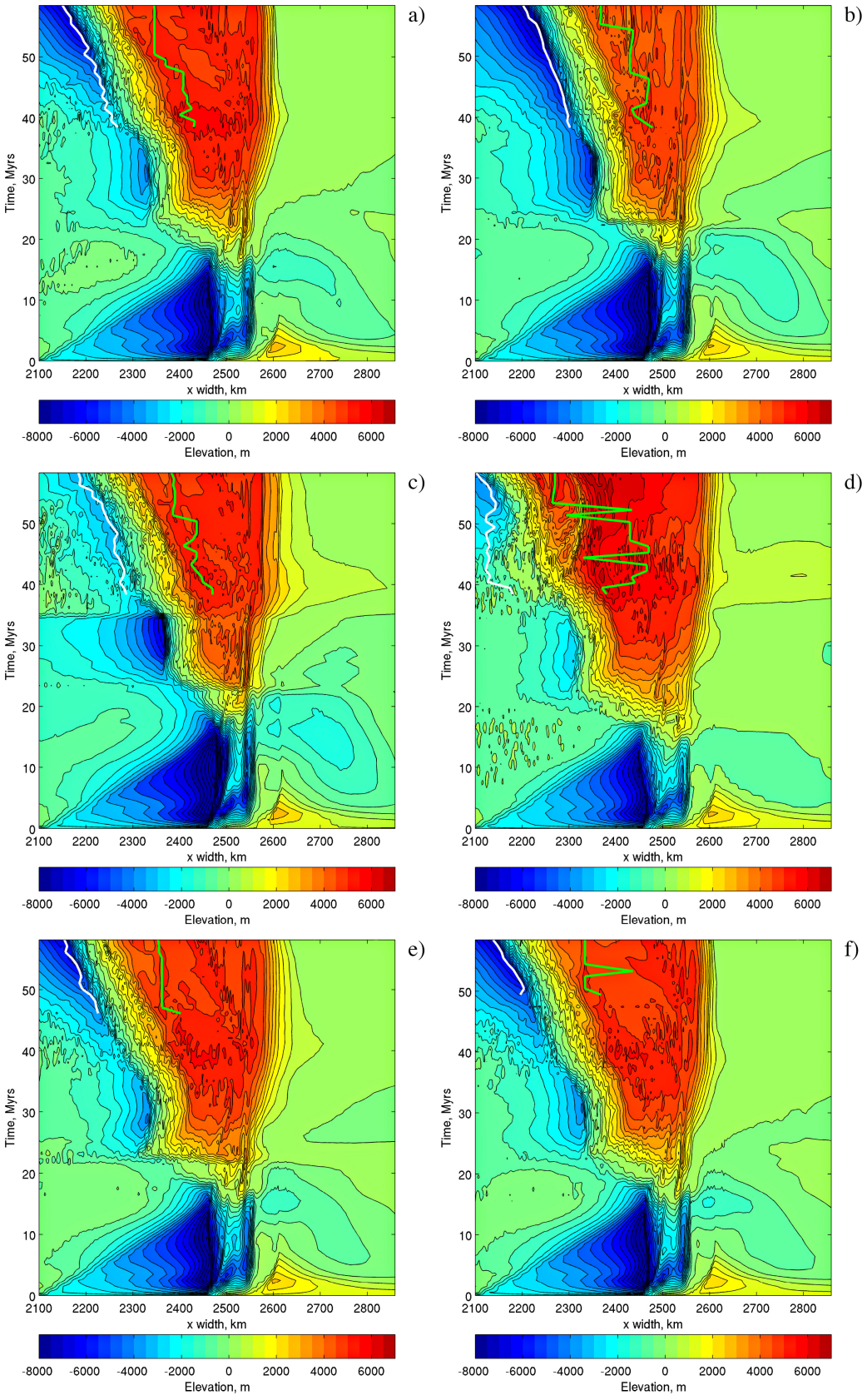
a)
b)
c)
d)
e)
f)
Time, Myrs
0
10
20
30
40
50
2100
2200
2300
2400
2500
2600
2700
2800
x width, km
-8000
-6000
-4000
-2000
0
2000
4000
6000
Elevation, m

Fig. 3.16: Comparison between the topography counturing of asymmetric models. In each figure there are two lines: white represents the migration of the topographic minimum during the simulation; green represents the migration of the topography maximum:the region of space bounded by these two lines is where the focused erosion acts. a)TestC3Mon'$_{c1}$; b) TestC3Mon'$_{c1s1}$; c)TestC3Mon'$_{c1s2}$;d) TestC3Mon'$_{c1s3}$; e)TestC3Mon'$^{45Ma}_{c1}$; f)TestC3Mon'$^{50Ma}_{c1}$

TestC3Mon'$_{c1}$ and t$_{mon}$

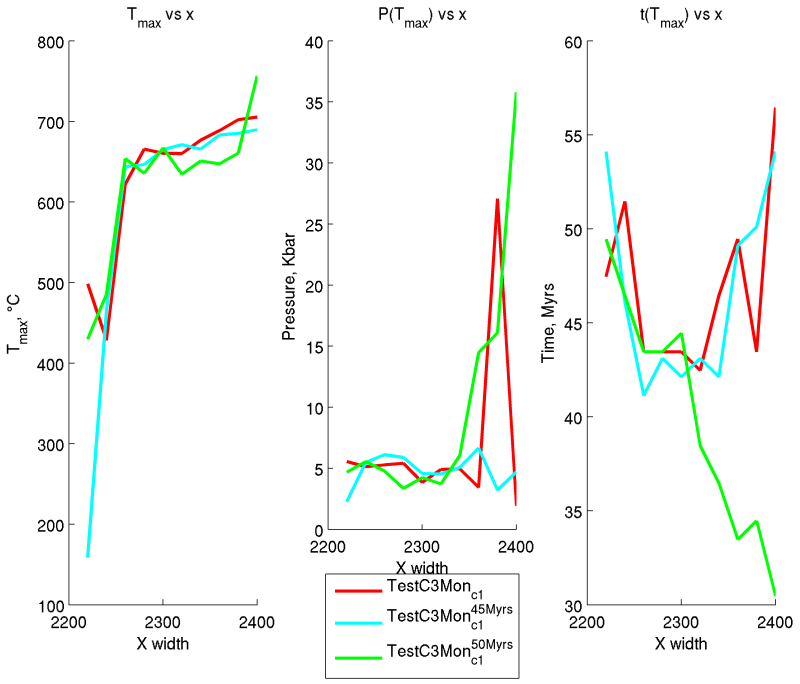

Fig. 3.17: Left:T$_{max}$ against x ;Centre:P(T$_{max}$) against x: In TestC3Mon'$^{50Ma}_{c1}$ pressure increases toward the centre of the orogen; Right: t(T$_{max}$) against x: In TestC3Mon'$^{50Ma}_{c1}$ the timing of the metamorphism decreases toward the centre of the orogen

This two simulation does not show any difference in the evolution of the orogen. The main observable difference is the different shapes of the partially melted region:

- TestC3Mon$_c1^{45Ma}$: the shape of the partially melted region is elongated toward the left foreland basin. Taking as reference the TestC3Mon$_{c1}$, dome-like structure in this simulation is shifted towards the right(see Fig. 3.18a).

- TestC3Mon$^{50Ma}_{c1}$:the shape of the partially melted region is triangular. The dome-like structure is shifted toward the right in respect with the position of the dome-like structure of the TestC3Mon'$_{c1}$(see Fig. 3.18 b).

The position of the dome-like structure, and the shape of the partially melted region seem to be affected by the focused erosion. The duration of focused erosion affects the dynamics of the partially melted channel.

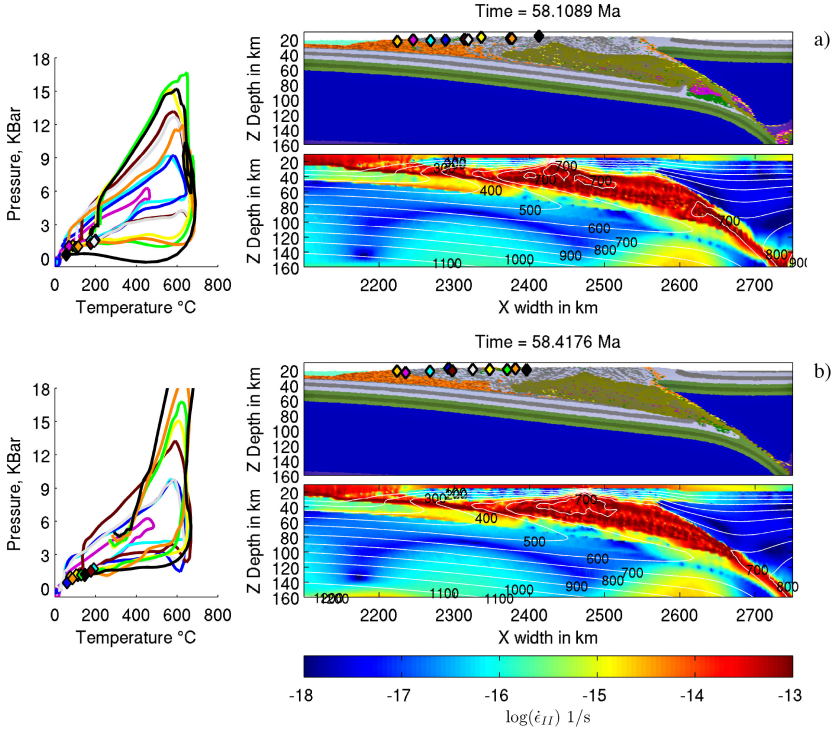

Fig. 3.18: Last time step of: a)TestC3Mon'$^{45MA}_{c1}$; b) TestC3Mon$^{50MA}_{c1}$

TestC3Mon'$^{45Ma}_{c1}$ does not show any difference with the reference model. The main features of the reference test are preserved, so, the exhumation mechanisms is equivalent. On the other hand TestC3Mon'$^{50Ma}_{c1}$ has many difference (see Fig. 3.17):

- The P(T_{max}) augments with the structural level;
- The t(T_{max}) diminishes with the stuctural level.

The upper structural level has achieved higher pressure than the lower and the timing of maximum metamorphic grade registered of the global section considered is diachronous and follow a specific pattern. This behavior can be considered similar to the one proposed by Montomoli [Montomoli et al., 2013, Montomoli et al., 2014] for the Himalaya.

Topography does not show first order difference with respect of the reference model. Corrugation decays with time and the position of the dome-like structure can be observe in its surface manifestation. The dome-like structure migrates to the left, and its final position depends on the initialisation of the focused erosion.

Therefore the corrugation of the plateu are more sharp in the region beyond the dome-like structure(see Fig. 3.16 e,f).

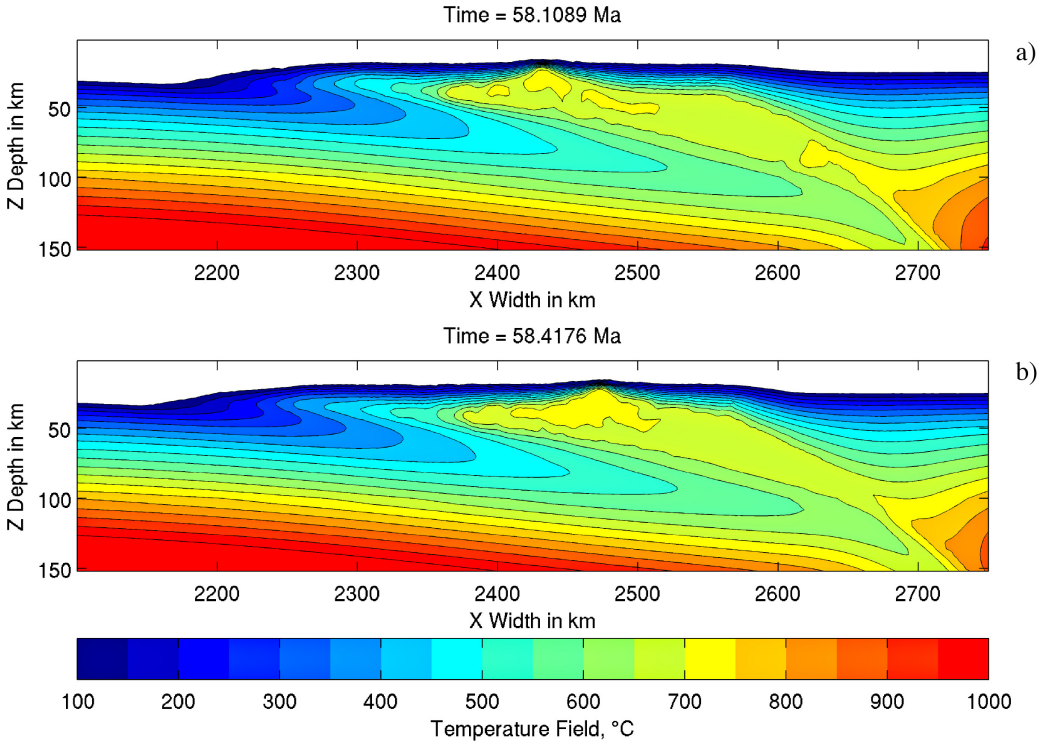

Fig. 3.19: Countouring of the final temperature field: a)TestC3Mon'$^{45MA}_{c1}$; b) a)TestC3Mon'$^{50MA}_{c1}$.

Chapter 4

Discussion

4.1 Limit of the simulation and future perspectives

4.1.1 Partial melting

In my simulation the melt segregation processes are not considered, although they play an important role in the development of the crustal differentiation and in the evolution of the rheological properties of the melting rock. Therefore, the simulation results are indicative of the first order behavior of the orogen. For example, the segregation of melt during the emplacement of the Great Himalayan sequence have produced the leucogranites pluton [Vanderhaeghe, 2009].

The discussion of results starts from the partial melt processes which have a primary role in the development of my models. The first issue to discuss is the viscosity and buoyancy of the partially melted rocks. Rocks which partially melted are characterised by relatively low viscosity and low density with respect to the unmelted counterpart. The partially melted rocks influence the development of the orogenic belt [Vanderhaeghe, 2009], not only with respect to the crustal differentiation, but also for the distribution of the strain in the orogenic belt [Vanderhaeghe, 2009]. On the one hand, the buoyancy of the partially melted rocks increases the strain in the vertical direction; on the other hand, the lateral variation of crustal thickness and topography produces horizontal pressure gradients, yielding to horizontal channel flow [Avouac and Burov, 1996, Burov and Toussaint, 2007, Beaumont et al., 2004].

The rheological behavior of partially melted rocks is complex and depends on M

(volumetric degree of melting), strain rate and distribution of the melt through the rocks [Vanderhaeghe, 2009, Caricchi et al., 2007]. The rheology of partially melted rocks is the same of the unmelted rocks until it reaches a critical value of melt fraction M = 0.1. Above this critical value, the viscosity of partially melted rocks is calculate using the equation (eq.(2.34)), that is representative of crystalline suspensions [Bittner and Schmeling, 1995, Pinkerton and Stevenson, 1992]. However equation (eq.(2.34)) does not simulate the dependency to the applied strain rate and stress that has been shown to exist for M $<$ 0.4 [Rosenberg and Handy, 2005]. This implies that the simulated mechanical behavior of the might not be fully representative of the partially melted rock deformation.

4.1.2 Metamorphic reactions

The metamorphic reactions and phase transitions are difficult to deal with the continuum mechanics approximation, because they change suddenly the mechanical-thermical-physical properties of the rocks. The implementation of this kind of processes is one of the major task of the numerical modelling [Gerya, 2009].
The absence of these reactions produces several problems in reproducing the continental collision processes. Burov argued that the continental subduction processes may be facilitated by the metamorphic reactions, because they produce weak rocks which lubricate the subduction interface [Burov et al., 2014]. The weakening processes associated with metamorphic reactions in the simulation performed for this thesis processes are not taken in account. This places an important limit of my models which solely respresent first order feature of the orogenic processes.
One of the future perspective is to improve the ability of the numerical code to deal with metamorphic reactions and investigate the way in which they affects the development of the orogenic belt.

4.1.3 Transport Equation

Another important simplification of the simulation is associated to the rheological properties of the sediments created by the transport equation which are the same of the sedimentary rock (even the radiogenic heat production is the same). The rheol-

ogy of unconsolidated sediments may not play a first order role in the development of the orogens, but, on the other hand the radiogenic heat production may induce first order modification of the evolution of the orogen. For example, the heat produced by the radiogenic sediments induce thermally relaxation in the underthrusting U.C., which may buckle (see Fig. 3.13). So, a fundamental question is if the sediments produced by erosion can have similar radiogenic heat production of the sediments source. The radiogenic heat production is associated with the concentration of radiogenic elements:U,Th and ^{40}K. These elements are highly sensitive to dissolution, therefore the weathering process may remove radiogenic elements from the sedimentary rocks and the crustal rocks [Vilà et al., 2010]. Apart from the fact the numerical technique have not the ability to resolve in detail the natural variability of the rocks physical properties, the question about the radiogenic heat production of the sediment producted by surface processes is still valid. In any case the high radiogenic heat value has been measured in the sediments [Faccenda et al., 2008]. It is necessary to investigate if the usage of different kind of sediments produced by erosion may produce secondary or first order feature on the development of the simulation.

4.2 Asymmetric models as numerical analogue of Himalayan orogenetic belt

Bearing in mind all the previously discussed limitations of the used numerical approach, the simulation performed during this thesis project may be confronted with real orogenic system. As I mentioned in the section 1, as the paradigmatic case study of hot orogens is the Tibetan-Himalayan system [Beaumont et al., 2006, Beaumont et al., 2010], all the simulations were with the aim to reproduce a model which can be compared with the Himalayan range.

4.2.1 Basic geological background of Himalayan Range

The Himalayan orogenic system is one of the best example of orogen created by continent-continent collision [Yin and Harrison, 2000, Yin, 2006]. The Himalayan

range is still active and the incredible exposure of the tectono-stratigraphic unit make it one of the best place to describe the processes involved in the mountain building [Yin, 2006, Montomoli et al., 2013]. Despite these advantages, the literature of the Himalayan range is often confusing and the lack of a common perspective produces several difficulties in the interpretation of the Himalayan range [Yin, 2006]. Even if several structures have an incredible continuity along the strike of the mountain chain, the geometry of the structure, the displacement along them, and last but not least the lithology along the main tectonic structures continuously vary along the strike [Yin, 2006]. The main problem of many studies related to the tectonic evolution of the Himalayan range is associated with the fact that often local features are used to extrapolate the dynamics of the whole orogenetic system [Yin, 2006].

Geological Background

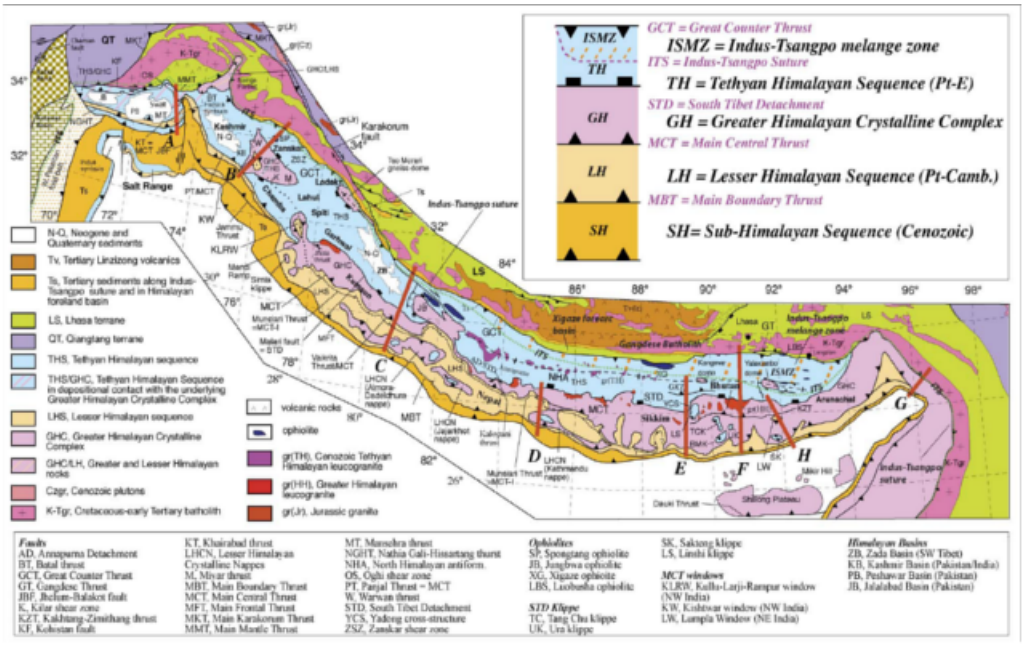

Fig. 4.1: Geological map of Himalaya [Yin, 2006]

The Himalayan range is a wide mountain chain. It extends in the northern India from the west to the east, its length is 2500 km. The geomorphological limit of the orogen is defined by the left-flow Indus river and the right-flow Yalu-Tsangapo river in the north, by the limit of the ghangetic depression in the south (this limit is defined by the Main Frontal Thrust, MFT) and by the Namcha Barwa and Nanga Parbat peaks in the east and west, respectively [Yin, 2006].

The Himalayan orogenetic system is delimited by four megascopic structures: the

Indus-Yalu-Tsangapo structure in the north, the left slip Chaman fault in the west, and the right slip Sagaing fault in the east, while the southern border of the orogenetic system is defined by the Main Frontal Thrust [Yin and Harrison, 2000, Yin, 2006].

The tectono-stratigraphic subdivision is one of the most interesting issues of the Himalaya. The classic subdivision assumes that there are four main tectonic stratigraphic units bounded by four structures, which are continuous along all the Himalayan Range [Heim and Gansser, 1939].

- Sub-Himalaya tertiary strata: sedimentary rocks deposed during the Tertiary.
- Lesser Himalayan (Lesser Himalayan Sequence or Lower Himalayan, LHS): low grade metasedimentary rocks or unmetamorphosed sedimentary rocks. The age of the rocks belonging to this tectono-stratigraphic unit spans from Proterozoic to Cambrian [Yin and Harrison, 2000, Yin, 2006] .
- Great Himalayan Sequence (Great Himalayan Crystalline Complex, GHS): the lithology of this unit varies along strike: in north Pakistan the rocks are unmetamorphosed and indistinguishable to the Tethyan Himalayan Sequence,while in the centre and in the eastern part of the Himalaya this unit is composed by high grade metamorphic rock. The main feature of the metamorphic core complex is the inverted metamorphic gradient in the lower part of the crystalline sequence [1]. From the middle of the unit to the South Tibetan detachment the metamorphic gradient is normal. The age of the rocks spans from the Paleproterozoic to the Ordovician [Yin, 2006, Montomoli et al., 2013]. The following section will introduce all the characteristics of the GHS.
- Tethyan Himalayan sequence (THS): sedimentary rocks (siliciclastic and carbonate). The age of the rocks spans from the Paleoproterozoic to Eocene. The lithology varies along and perpendicularly to the Himalayas [Yin, 2006].

All the units are bounded by the four main faults:

- Main Boundary Thrust: thrust that places the LHS sequence above the Sub-Himalayan sequence [Yin and Harrison, 2000, Yin, 2006].

[1] inverted metamorphic gradient: the metamorphic gradient augments toward the higher structural level

- Main Central Thrust: this thrust is defined as the shear zone that places in contact the LHS with the GHS [Yin and Harrison, 2000, Yin, 2006].
- South Tibetan Detachment: this normal shear zone (?)[2] defines the contact between the THS and GHS [Yin and Harrison, 2000, Yin, 2006] .
- Indus-Yalu-Tsangapo Suture: the suture zone is the northern limit of the Himalayan orogenic system.

This geographical and geological subdivision does not take in account the variability along strike of the geometry of the structure, and the variability of the lithology of these four tectono-stratigraphic units [Yin, 2006, He et al., 2014, Webb et al., 2011]. The geometry of the MCT is complex, and varies along the orogen. The classical definition is based on the lithological difference between the hanging-wall and footwall rocks [Yin, 2006]. This definition is not valid in all the orogen, because the Main Central Thrust cuts the tectono-stratigraphic unit described above [Yin, 2006]. The MCT and STD are considered parallel structures. This assumption is not completely correct, because at places MCT and STD merge into a unique structure [Yin, 2006, He et al., 2014, Webb et al., 2011]. In spite of the along strike variability of the geometry of the main structures, this subdivision perfectly fit the central Himalayan structural setting [Yin and Harrison, 2000].

4.2.2 Great Himalaya Sequence, Main Central Thrust and South Tibetan Detachment: exhumation model and evolution of the Himalayan system

Great Himalayan Sequence as coherent unit, Main Central Thrust, South Tibetan Detachment activity

The GHS has been considered a coherent unit [Beaumont et al., 2001, Beaumont et al., 2004, Grujic et al., 1996, Yin and Harrison, 2000] cutting the surrounding units by means of out of sequence thrust [Montomoli et al., 2014, Imayama et al., 2012].The GHS is mainly composed by medium to high grade metamorphic rocks: upper amphibolite-grade shist, gneiss and migmatites [Montomoli et al., 2013][3].The

[2]The sense of shear is complex, there is not an univoque interpretation of the structural data.
[3]all the peak metamorphism data are described in the 'paradigms shift section'

unit is intruded by several leucogranites plutons (High Himalayan Leucogranites), which are associated to the migmatitic gneiss [Visona et al., 2012]. This unit has been regarded as coherent unit, consequently all the models that have tried to explain its emplacement have had as fundamental postulate the coherence of the GHS [Montomoli et al., 2014]. The interpretative models that have been produced in the last decades have considered the STD and MCT as the main protagonist of the emplacement of the GHS. Hence, a discussion about these two structures is needed. The geometrical variability of the structure cited in my work is not the main topic of my thesis project, and the main kinematic and exhumation model proposed for the Himalayan range are made upon the observation of the central Himalaya (Nepal). Consequently, for the sake of the simplicity, I will principally refer to the geometry find in this region of the Himalaya.

- **Main Central Thrust**: in the central Himalaya the MCT is a shear zone, its thickness spans from 2 km to 10 km [Yin, 2006]. In Nepal, MCT has a flat-ramp geometry. The foliation of the GHC above the ramp geometry dips to the north [Yin, 2006], and the material transport is toward the south [Yin and Harrison, 2000, Yin, 2006, Montomoli et al., 2013]. The age of the activity of the MCT varies from the north to the south [Yin, 2006]. The age of the MCT spans from 23 to 13 Ma (Montomoli 2014), with a final reactivation of the structure in the south from 8 Ma to 3 Ma [Yin, 2006].

- **South Tibetan Detachment**: STD juxtapose the THS above the GHS. It consists of several sub-parallel faults and shear zones with a complex motion history [Yin, 2006, Webb et al., 2011, He et al., 2014]. The alternating shear sense (top to the north, top to the south) is the main feature of the STD [Yin, 2006, Montomoli et al., 2013]. The age of activity of the STD is constrained by the age of undeformed leucogranites intruded in both the GHS and the THS [Carosi et al., 2013]. These leucogranites emplace at 23 Myrs.

Exhumation Models

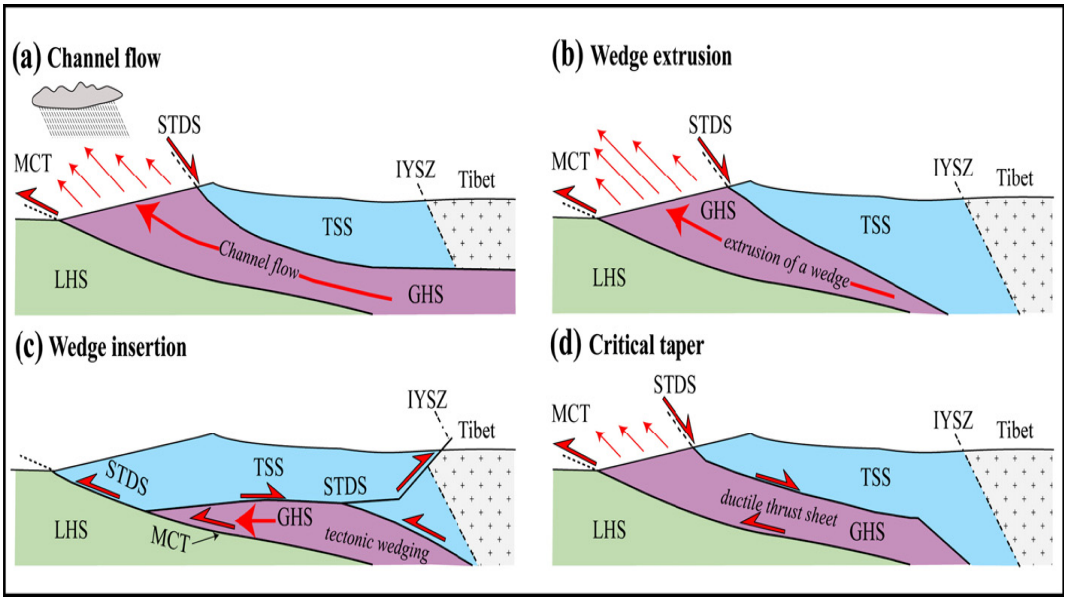

Fig. 4.2: Schematic representation of the exhumation model proposed. STDS: South Tibetan Detachment; MCT: Main Central Thrust; IYSZ: Indus-Yalu Tsaganpo suture zone; TSS: Tethyan Himalayan Sequence; GHS: Great Himalayan Sequence; LHS: Lower Himalayan Sequence, [Montomoli et al., 2013]

Several models have been proposed to explain the emplacement of the GHS. STD and MCT play a key role in all the models. Since the STD has an alternating sense of shear, the STD is interpretated as a back thrust or as an extensional shear zone. All the main models are shortly described(see Fig. 4.2). The channel flow model will be described more in detail in the following section, because it is very similar to my models:

1. **Wedge extrusion**: GHS extrudes as north-tapering coherent wedge. The extrusion of the wedge is accommodated by a combination of continuous extension along STD, and contraction along the MCT. There are several variation of this model as a function of the features ascribed to the GHS: a) rigid wedge [Hodges et al., 1992]; b) Ductile Wedge (Grujic 1996). The models requirements are not consistent with the activity of the two shear zones involved in the exhumation of the GHS.

2. **Wedge Insertion**:Similar to the Wedge extrusion, but the geometry of the wedge is south-tapering [Webb et al., 2007, Webb et al., 2011]. The main feature of this model is the interpretation of the STD as back thrust. This model arises principally from the fact that the STD and MCT merge in an

unique structure at the south [Yin, 2006, Webb et al., 2011, He et al., 2014].

3. **Coloumb Wedge**: the Himalayan orogenetic system is interpreted with the coloumb wedge theory [Kohn, 2008]. The shortening and the extension are alternating processes, and depend on the thickness of the wedge.

Channel Flow

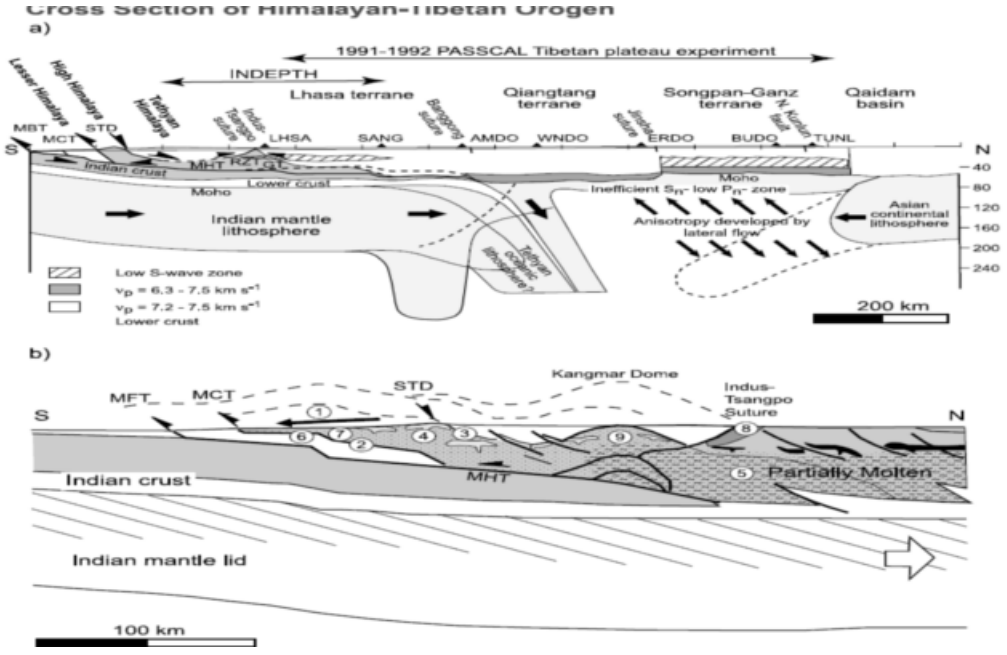

Fig. 4.3: Channel flow model, [Beaumont et al., 2004]

There are two channel flow models which have substantial different implications on the overall tectonic evolution of the Himalaya. The terminology used may lead to confuse the model proposed by Nelson, and the one proposed by Beaumont [Beaumont et al., 2001, Beaumont et al., 2004]. The model proposed by Nelson assumes that GHS is a coherent unit that comes from the Tibetan lower-middle crust [Nelson et al., 1996]. The tibetan crust in this model is transported to the southern flank by the mechanism of channel flow. This hypothesis is not correct : the GHS it is not an allocthonous unit, and belongs to the Indian crust [Yin, 2006].

The other model is the *Channel Flow* of Beaumont [Beaumont et al., 2001, Beaumont et al., 2004] (see Fig. 4.3). The model that emerges from the simulation of Beaumont is simple:

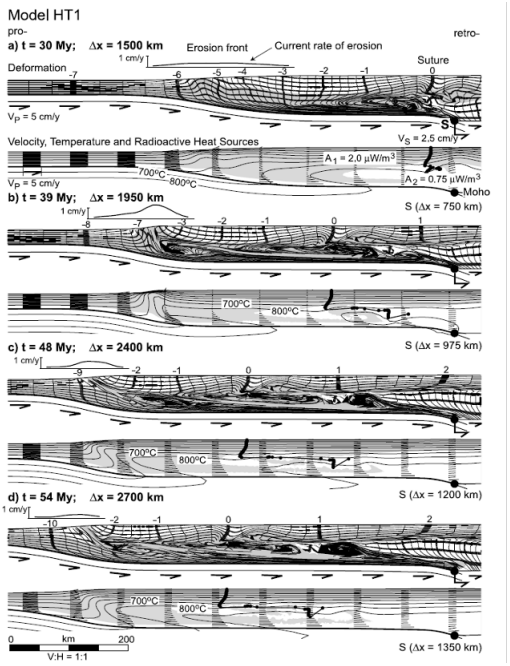

Fig. 4.4: Evolution of the Beaumont test from the initialisation of the focused erosion: Focused erosion value varies along the slope, and in time between 0-2 cmyrs^{-1}. In this particular test the S-point (the point in which the upper crust detaches from the lower crust) displace along x in order to simulate the subduction advancing.The Indian crust is underthrusted underneath the tibetan crust, where it is heated by radiogenic heat production. After the occuring of partial melting the indian melted crust starts to inverte its velocity field following the pressure gradient between the tibetan plateu and the southern flank. [Beaumont et al., 2004]

1. the Indian upper crust is under-thrusted beneath the Tibetan Crust;

2. the thickened crust heats up mainly by radiogenic heating;

3. due to the increase of temperature, partially melts. The frontal exhumation is caused by the focused erosion along the southern flank that modifies the pressure gradient and favour the flow field toward the surface [Beaumont et al., 2001, Beaumont et al., 2004].

As it is extruded, the partially melted crust cools and solidify. The melting processes and the return flow are caused by the weakening effect of the self heating processes, then the *conditio sine qua non* for the exhumation at the surface is provided by high focused erosion . I want to highlight that the upper-middle and partially melted crust flows toward the south in any case due to the horizontal pressure gradient. If the erosion is not so 'strong', the channel flow starts to tunnel and deform the converging indian crust at depth [Beaumont et al., 2001, Beaumont et al., 2004].

The erosion rate used for the simulations by Beaumont varies between 0-2 $cm\ yrs^{-1}$. These erosion rate are too high. The erosion rates of the Himalayan range are much lower, and show different spatial and temporal patterns, ranging from 0.8 to 2.7 $mmyrs^{-1}$ [Thiede and Ehlers, 2013, Vance et al., 2003]. Yin have pointed that the timing used for the focused erosion is not consistent with the denudation rate found in the Himalayan rocks and argued that the high denudation/exhumation rate begins 10 Ma ago [Yin, 2006].

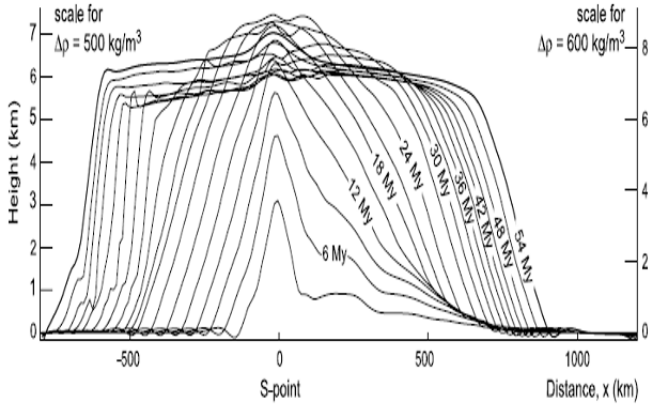

Fig. 4.5: Topography evolution of the Beaumont's simulation: the S-point is the subduction point in which the Upper crust is forced to detach from the lower crust. The topography evolution is similar to my simmetric model.

The processes described by Beaumont is similar to the injection of the L.U.C. in the symmetric models [Beaumont et al., 2001, Beaumont et al., 2004, Beaumont et al., 2006](see Fig. 3.7, Fig. 3.6). The topographic evolution is almost the same, the injected crust propagates toward the right and induces uplift toward the right. The main difference arises from the fact that the partially melted crust remains in the upper plate, and the propagation toward the left of the partially melted crust is blocked by the converging L.U.C. materials. In my models the L.U.C. injects between the R.U.C. and the R.L.C., the necessary condition of this behavior is the yielding of the R.U.C.. The counterflow of the partially melted crust, is weak and chaotic. As I mentioned before in the model produced by Beaumont [Beaumont et al., 2001, Beaumont et al., 2004, Beaumont et al., 2006] the channel flow always occurs. The difference of the several modes of channel flow produced by Beaumont depends on the efficiency of the surface processes [Beaumont et al., 2004, Beaumont

et al., 2006]. I have not tested the focused erosion in these model because the the paramount condition expresses by Beaumont does not happen:

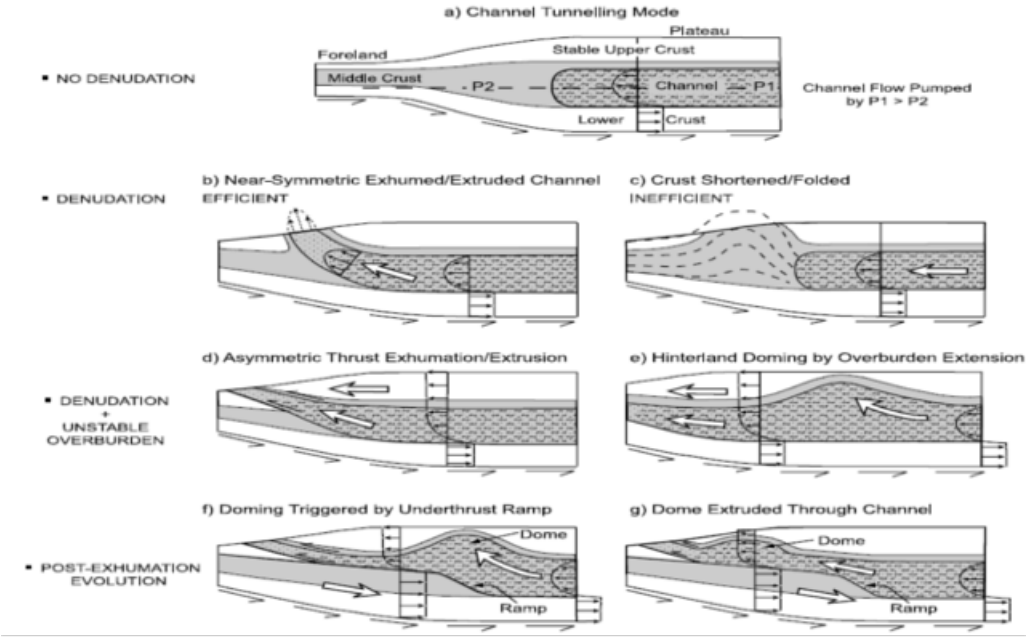

Fig. 4.6: Behaviour of channel flow in function of the denudation rate. [Beaumont et al., 2004]

the partially melted crust does not behave in the way predicted by Beaumont, and the counterflow is linked to the less ability of the L.U.C. to wedge into the R.U.C. and L.U.C. in the right plate. The simulation that I have performed reproduce the topographic feature of Beaumont's models(see Fig. 4.5 and Fig. 3.6).

4.2.3 Paradigm shift

The common postulate of all models is the coherence of the GHS. Consequently the models have focused only in the role played by the two shear zone that bounded the GHS [Montomoli et al., 2014]. The idea was renforced by the $^{40}Ar/^{39}Ar$ ages of white micas; this mineral have a low closure temperature, therefore the data cannot support the idea of the coherence of the units, but the idea of the coherent behavior at low temperatures of the GHS [Montomoli et al., 2014].

The detailed studies of the migmatites in the GHS and the associated leucogranites have demonstrated that there are two discontinuous events of partial melting [Imayama et al., 2012]. These multiple and discontinous partial melting processes are not compatible with the coherent channel flow models proposed by Beaumont [Imayama et al., 2012].

During the last years several tectonic-metamorphic discontinuities have been discovered in the GHS [Montomoli et al., 2013, Montomoli et al., 2014]. All the discontinuities have a top-to-the-south sense of shear, and the age of activity is older than the activity of the Main Central Thrust [Montomoli et al., 2014]. The hanging-wall and the footwall show different metamorphic grades: the hangingwall is characterized by lower peak pressures than the footwall; the metamorphism of the hangin-wall rock is older than the footwall. The widespread presence of this metamorphic discontinuities in the GHS is considered the expression of a regional scale structure, the High Himalayan Discontinuity (HHD) .

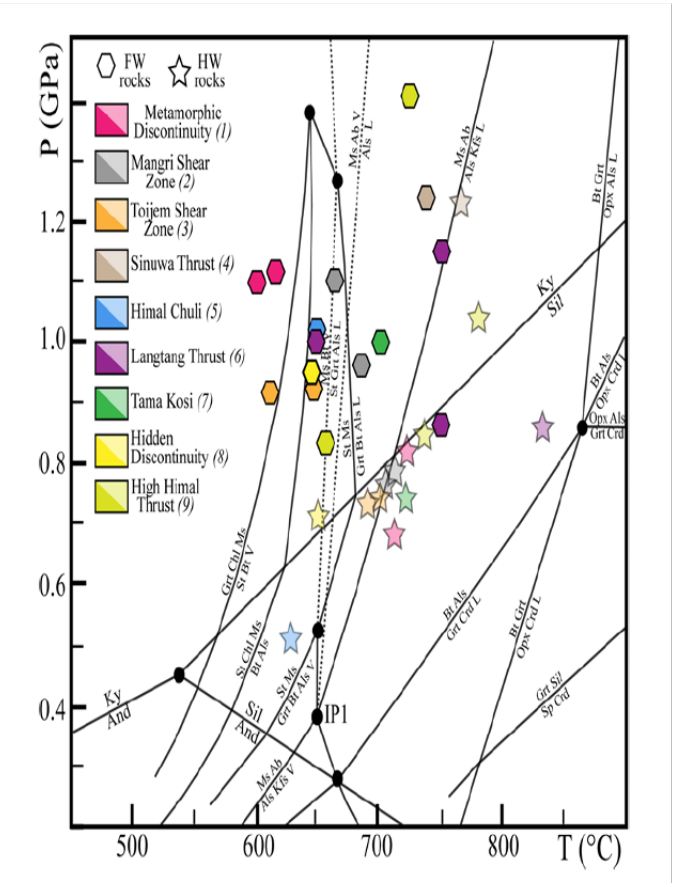

Fig. 4.7: Thermobarometric data from the metamorphic discontinuites [Montomoli et al., 2014]

HHD divides GHS into two different slice:

- GHS_{upper}: made of Ky-Sil migmatites with higher degree of melting. The maximum temperature achieved by the footwall on all the shear zone spans from 650-750 °C, with a metamorphic peak pressure that spans from 0.7 GPa to 1.25 GPa;

- GHS_{lower}: made of migmatites with lower degree of melting. The P-T condition are approximately in the Ky zone. The peak temperature spans from 630-750°C;

The activity of this regional structure is older than the main central thrust and spans from 26 Ma to 17 Ma [Montomoli et al., 2013, Montomoli et al., 2014, Carosi et al., 2010].

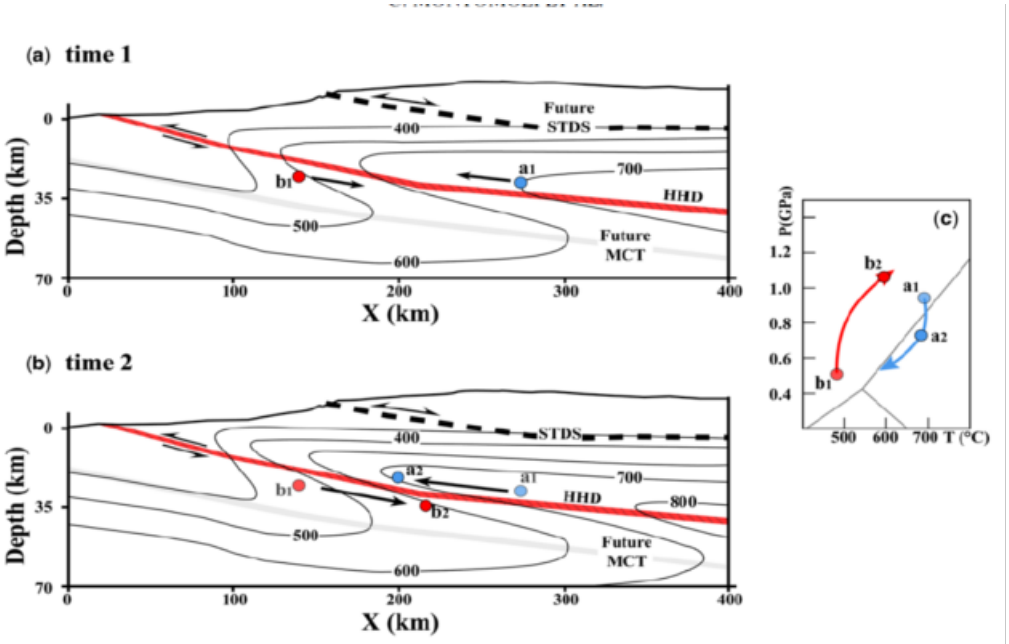

Fig. 4.8: Schematic representation of the new exhumation model proposed for the Himalayan range. [Montomoli et al., 2014]

The discovering of these tectono-metamorphic discontinuities is a turning point in the Himalayan research, because the metamorphic P-T-t path predicted by channel flow and in the other models is not consistent with the presence of other discontinuities in the GHS [Imayama et al., 2012]. The exhumation and burial patterns discovered in the GHS implies simultaneous burial and exhumation processes. Slices of crust are under-thrusted continuously, meanwhile the shortening shift toward the foreland. After the initialisation of a new shear zone, the rocks transported by the previous shear zone to high depths are heated and eventually partially melted, then they are exhumed. During the exhumation processes, the new shear zone transport other rock unit toward high depths (see Fig. 4.8) [Montomoli et al., 2013, Montomoli et al., 2014].

4.2.4 Discussion of the simulation results

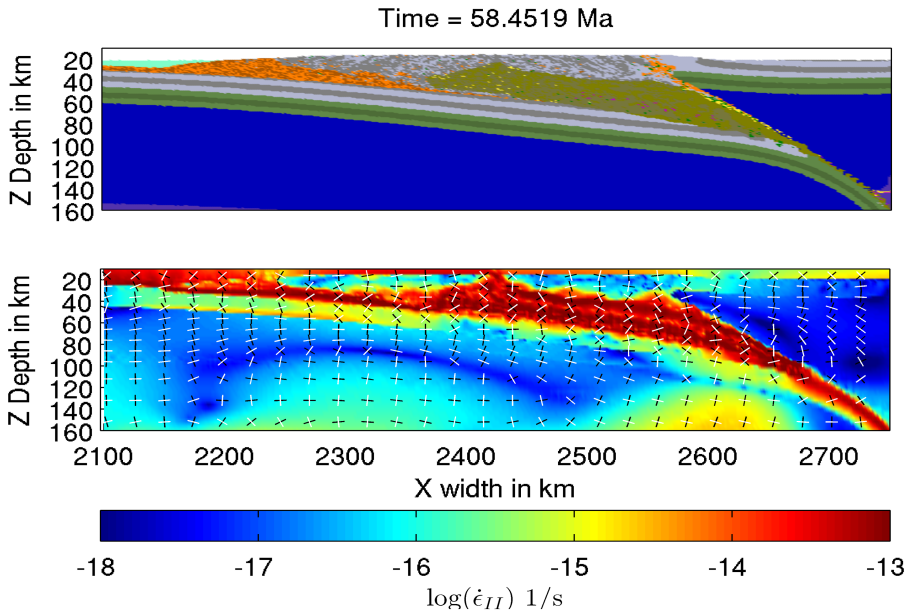

Fig. 4.9: This picture represents the final step of TestC3Mon'$_{c1}$. The upper figure is the composition map, the lower one is the $log_{10}(\dot{\epsilon}_{II})$ in which the principal axis of the stress tensor are plotted. The white represents the compression axis, the black represents the maximum extension achieved. The emplacement of the dome induce a localised extension in the brittle layer. The material flow induced by the dome like structure is faster than the far brittle layer which undergoes to compression at the right and left

The symmetric model have several shortcomings: the temperature is lower than the asymmetric models and the partially melted crust does not migrate efficiently toward the left foreland. Despite this, the symmetric models show sequential burial and exhumation processes migrating progressively toward the left foreland. The propagation of the shortening in the symmetric models does not migrate toward the left foreland, and the uplift is distributed between the left plate and the right plate. This kind of models shows similar characteristics to the model proposed by the Beaumont: the L.U.C. material that wedges in between the interface between R.U.C. and the R.L.C. self heats and partially melts. The behavior of the partially melted crust does not show the feature of the channel flow proposed by Beaumont. Summarising, the symmetric models do not well represent the Himalayan range.

The asymmetric models have the necessary condition to be considered the numerical analogue of the Himalayan range. In all simulations, there are several structures that can be associated with the principal Himalayan range faults. The main décolement surface can be considered as the Main Frontal Thrust, while the faults that

place in contact the deformed, frontal sedimentary sequence and the metamorphosed U.C. can be considered a structure similar to the Main Central Thrust. As I have mentioned in section 3.3 the L.U.C. can be divided into three sub-domains: u.U.C. which is the strong upper crust that is underthrust underneath the montain range; the low viscosity channel mainly composed by U.C. composition rocks; upper brittle layer. In all the asymmetric simulations (except for TestC3Mon'$_{c1s3}$) the uppermost brittle layer experiences extensional tectonics in the interior of the orogen and compressional tectonics on the left flank. The temperature in the simulated orogens is high but, except for the reference model (TestC3), it is lower than the temperature achieved by the Himalayan range [Montomoli et al., 2013, Montomoli et al., 2014, Imayama et al., 2012]. In most of the performed simulations dome-like structures emerge; the dome-like structures are similar to the gneissic dome in Himalayan range [Zhang et al., 2012]. The North Himalayan Gneissic Dome (NHGD) is a discontinuous belt in the north of the Himalaya. According to [Zhang et al., 2012], the formation of the NHGD is associated with the activity of STD, which induce a decompression and then trigger the upwelling of the partially melted materials.

The main difference of the asymmetric models and the model proposed by Beaumont, is linked to the focused erosion [Beaumont et al., 2004, Beaumont et al., 2006]: in my models the channel flow mode exists in any case, for lower erosion rates and for higher erosion rates. The parameter that affects the style of the crustal deformation and allows the tunneling mode is the sedimentation rate. The high radiogenic sediments heat and weaken the L.U.C., which buckles(see Fig. 3.13). Since the convergence rate imposed is constant, the buckled L.U.C. evolves into a megathrust. Beaumont associate this behaviour to the low erosion rate [Beaumont et al., 2004, Beaumont et al., 2006].

The timing of the initialisation of the focused erosion affects the shape and influences the partially melted region. In the models in which the partially melted region is wider and affects the exhumation processes, the timing of the T_{max} does not show any pattern with respect to the structural level(see Fig. 3.18).

All the simulations performed in this thesis are characterised by an inverted metamorphic gradient with P(T_{max}) and T_{max} ranging from 150°C to 700 °C, and

from 2 to 15 Kbar[4], respectively. The sequentially burial and exhumation processes are principally associated to the symmetric models and to TestC3Mon$_{c1}^{50Ma}$, while in the asymmetric models this feature is not observed.

In TestC3Mon$_{c1}^{50Ma}$ Lagrangian particles show a similar metamorphic gradient of the symmetric models(see Fig. 3.17). The timing of the high-grade metamorphism diminishes toward the centre of the chain. The Pressure at T$_{max}$ does not show any pattern with respect to the structural level for all the models. On the other hand, the absolute maximum pressure increases toward the interior of the orogen or all the models.TestC3Mon$_{c1}^{50}$ show similar temperatures to the GHS metamorphic rocks, and show similar peak metamorphic ages pattern of the rocks of the models proposed by Montomoli and Carosi [Montomoli et al., 2014, Carosi et al., 2010].On the other hand, the pressures achieved by the selected Lagrangian markers do not show one of the key feature of the new model proposed by Carosi and Montmoli : the Lagrangian particles of the higher structural lever have not a lower pressure than the lower ones. I envisage that the evolution model proposed by Montomoli and Carosi, [Montomoli et al., 2014, Carosi et al., 2010], needs to be simulated with a visco-elasto-plastic rheological model, because the rheological constitutive model used in the presented simulations cannot easily reproduce localized deformation along shear zones.

The partially melted rocks have a lower density than the country rocks. The body forces acting on p.m.U.C. are strong, consequently the Lagrangian markers that undergoes melting are faster, owing to also their relatively low viscosity. In all the simulations presented the buoyant p.m.U.C. forms dome-like structures. The dome-like structures are closely associated with the region of the partially melted rocks with the highest temperature, where the buoyancy force are the highest. The emplacement of the dome-like structure is associated with extensional tectonics, which can be observed in the development of the topography images . The brittle layer of the orogenetic system in the asymmetric models experiences alternating phase of extension and compression as the extensional domain associated to the dome-like structure migrates toward the left(see Fig. 4.9). The dome-like structure position is sensitive to the timing of the focused erosion: the focused erosion forces the advection of L.U.C. towards the left, consequently the hot materials is advected

[4]UHP Lagrangian markers are excluded

with L.U.C. materials toward the left. The advection induces a displacement of the temperature field, consequently the highest temperature zone is shifted toward the left. If the focused erosion starts in the final stage of the simulation, the advection of the hot material is inhibited.

Channel flow like behavior emerges only if the R.U.C. acts as an efficient (i.e., mechanically strong) backstop. The focused frontal erosion affects the channel flow dynamics, but it is not indispensable to the exhumation of the channel flow. On the other hand, the sedimentation affects the first order feature of the simulation and the tunneling mode of propagation of the channel flow emerges if the U.C. is thermally weakened.

Chapter 5

Conclusion

The main aim of this thesis is to investigate the behavior of hot orogens. The Himalayan orogenetic system is the best example of hot orogens. The widespread presence of migmatites and the associated leucogranites testifies the occurrence of melting processes in the Himalayan range. The consequence of the presence of partially melted crust is an intriguing issue. Since the partially molten rocks have low viscosity and low density, they are highly sensitives to the variation of the topographic relief due to surface processes and to the applied stress.

The recent researches have focused on the possibility of the coupling between tectonics and surface processes. Tectonics may affect the atmospheric circulation and focus the precipitation in the flank of the uplifting mountain. Despite the fact that this assertion is logic and valid, the tectonic response to focused erosion or to surface processes is not yet understood. The field data are insufficient to discriminate the contribution of the surface processes to the uplifting or to the development of the geologic structure, and the tectonic processes themselves. From a theoretical perspective, the surface processes produce a variation of the loading in space and in time: this implies that the geologic structure may be affected by erosion and sedimentation, because they alter the stress field. Burov argued that the surface processes may promote thrust reactivation and may produce pressure gradient between two places that induce a ductile crustal flow underneath the surface [Avouac and Burov, 1996,Burov and Toussaint, 2007] The focused erosion is one of the necessary condition of the channel flow of Beaumont, because it alters the velocity pattern inducing the low viscosity channel to deflect toward the region in which the focused

erosion occurs. Himalayan has been regarded as one of the best place to test the hypothesis of the coupling between surface processes and the tectonics processes. As I previously mentioned, the Himalaya is characterised by the widespread presence of migmatites and leucogranites: the partially molten rocks are more sensitive to the variation of the pressure condition and due to their intrinsic mobility they may be affected by the surface processes.
My thesis work is focused on this specific issue: the mobility of partially melted rocks and the surface processes, and its consequence on the burial and exhumation processes.

5.1 Channel Flow necessary condition

Bearing in mind all the limitations of the simulations described in the discussion chapter, the first conclusion is linked to the condition of the channel flow like behavior and its exhumation: the channel flow like behavior emerges only in tests in which the Upper plate Crust is sufficiently strong to bear the stress arising from the collision. If these crustal units are weak, the lower plate crustal material injects in between the R.U.C. and R.L.C.. This produces a distributed thickening along the orogen and a migration of the uplift toward the right. The partially melted rocks start to migrate toward the left foreland in the final stage of the simulation because the injected material is stopped by the strength of the colder crustal unit of the retroforeland on the right plate. The temperatures achieved are low, and the partially melted rocks are not exhumed in the left flank. As a main conclusion, the crustal strength of the upperplate is a paramount condition for the emergence of high partially melted rocks and for the migration of the partially melted rocks toward the left flank.

5.2 Channel Flow and surface processes

The necessary condition to the apparence of the channel flow like behavior is the strength of the crust. The exhumation of the partially melted crust is not depen-

dent to the focused erosion: without this kind of erosion, the partially melted rocks are exhumed anyway. The surface processes affect the shape and the displacement of the partially melted zone. By testing independently the sedimentation rate, the timing of the focused erosion (and the erosion itself, these simulations are not shown in the thesis), the comparison between the results of several simulations show that it exists a first order variation in the development of the orogenetic system and in the exhumation pattern.

In tests where the channel flow is the major driving force of the exhumation process, there is not a systematic variation of the timing of the metamorphism with respect to the x position: the pattern is homogenous. On the other hand, the $\text{TestMon}_{c1}^{50Myrs}$ shows similar feature of the symmetric test: sequential burial and exhumation, and definite diminishing trend across the orogen of the timing of metamorphism. The partially melted region in $\text{TestMon}_{c1}^{50Myrs}$ is localized and quite stationary. Therefore I can argue that the focused erosion as well as the sedimentation rate promotes the advection of the partially melted region, and the most critical parameters to the advection are the timing of the focused erosion.

The sedimentation rate affects the orogenetic style more dramatically, if high sedimentation rate is used, the L.U.C. is weakened and the pure shear thickening and folding mode of deformation becomes the dominant mechanism of the deformation. This produces crustal buckling which evolves into mega-thrust. The localisation of deformation is associated with a moderate to high production of shear heating. This behavior is similar to the one predicted by Burg and used to explain the formation of the Himalayan syntaxis. This process is caused by the high radiogenic heat production of the sediments. The partially melt region after the development of the buckled crust starts to tunnel it. The sediments affect the orogenetic style with more intensity than the focused erosion. The sedimentation rate affects the rheological properties of the décolement surface because it provides sufficiently weak material to promote the material transport beneath it, but, on the other hand, the positive effect of the sedimentation rate disappears if higher sedimentation rate is used. There are two conclusions:

- the focused erosion cannot affect the channel flow in the way predicted by the Beaumont models;

- Sedimentation rate has higher effects on the orogenetic style than the erosion.

The main problem associated with this conclusion is the nature of the processes of sedimentation and erosion implemented in the code: sedimentation is independent from the erosional processes. This independence of the processes can be easily justified with the effects of the fluvial transportation in the third dimension; but I think that the way in which the surface processes are simulated has to be improved in order to achieve a better rendition of the natural system.

By means of these considerations and conclusions, I would like introduce the conclusion regarding the Himalayan range. The recent research on the GHS has shed a light on the real behavior of the mechanism of burial and exhumation of the GHS. This paradigm shift collides with the most popular model, the channel flow proposed by Beaumont. Taking into account all the limitations of my simulations, the most important point is the role of timing of the focused erosion. If t_{mon} value is low (the focused erosion acts for a longer period of time), the channel flow becomes the dominant process of exhumation. On the other hand, with higher t_mon (the focused erosion acts for a shorter period) the channel flow is not the dominant way of exhumation and burial and the exhumation pattern is similar to the behavior predicted by Montomoli. Following this conclusion, the logical consequence is that , the advection of partially melted crust did not play a primary role in the development of the GHS. The exhumation mechanism of GHS might be similar to the one proposed by Montomoli: the structure of the mountain range controls the exhumation. However, in my simulations this particular situation emerges by using a high value of t_{mon}. The simulation give a partial view of the reality, not only for the difference between my numerical experiment and the Himalayan chain, but also for the rheological model used for the description of the rock behavior. For example, in the simulation in which a visco-plasto-elasto rheological model is used, the effect of the surface processes is variable:

- discrete shifting toward the foreland of the thrust front;
- retreating behavior of the trench ;
- amount of the continental subduction [Burov and Toussaint, Toissaint].

Therefore, even if the exhumation pattern of $TestC3'Mon_{c1}^{50Ma}$ is similar to the prediction of Montomoli, this particular behavior arises from the variation of the timing of monsoonal erosion. Consequently the only conclusion possible is that the channel flow behavior is less compatible to natural observation. The reason why the channel flow behavior is inhibited cannot be deeply examinated with the used rheology law.

Acknowledgments

Finalmente posso liberarmi dalla pesantezza del linguaggio inglese per esprimermi al meglio delle mie possibilità, che sono comunque basse, ma tralasciamo questi dettagli. Non sono abituato a fare ringraziamenti stucchevoli, o comunque, usare le canoniche proforma di ringraziamento, perché non appartengono di certo al mio personaggio. Però, provo a fare uno strappo in onore di chi mi ha guidato e mi è stato vicino in questo interminabile percorso universitario.

La mia tesi è stata segnata da un incredibile serie di sfortunati eventi, che hanno reso questo percorso abbastanza parodistico. Tra i vari tentativi di suicidio del mio, fortunatamente vecchio, computer e varie cose che esplodevano a caso di certo non posso dire che durante questo percorso di tesi non abbia ricevuto una buona dose di emozioni. Prima di tutto ringrazio ufficialmente coloro i quali hanno deciso che non valeva la pena denunciarmi per stalking. Il primo che ringrazio è sicuramente il mio relatore Manuele Faccenda per avermi iniziato alla modellizzazione numerica, per avermi assistito durante la realizzazione della tesi e soprattutto per l'infinita pazienza portata. La seconda tornata di ringraziamenti va sicuramente a chi mi ha dato un continuo supporto linguistico durante la scrittura della tesi: Moreno Clementi, Pietro Mazzarol e Micheal (di cui non ricordo il cognome). Last but not least, devo ringraziare specialmente Davide Bettio, per avere salvato tutti i dati della mia tesi quando il mio computer ha deciso di morire in una triste giornata autunnale, e Davide Scot, il quale mi ha aiutato a modificare la funzione di matlab fnplot [1] permettendomi di fare dei bellissimi P-T-t path colorati. Infine ringrazio anche Luca Dal Zilio per avermi spacciato degli articoli scientifici di contrabbando. Ringrazio infinitamente anche Chiara Masiero per i consulti grafici, cioè, le immagini

[1] funzione molto carina che mi ha permesso di fare dei bellissimi P-T-t path, ma che non aveva implementata la capacità di seguire una mappa di colore rendendo di fatto la sua bellezza estetica inutile ai fini pratici

sono intelleggibili grazie a lei, nel senso che non riuscivo a gestire il foglio di inskape in modo tale da creare un pannello di immagini visibilli, carino.
Ora passo a ringraziare tutte le persone che mi sono state vicine durante quest'ultimo periodo, primo fra tutti Davide Contato che con un infinita pazienza mi ha sempre spronato a non abbattermi e mi ha ascoltato nei miei momenti peggiori, grazie infinite! Poi, di seguito, come promesso, ringrazio il gruppo di geologia strutturale HAPG con cui ho passato uno splendido periodo universitario che non dimenticherò mai, rinchiusi in quello che potrebbe essere definita la nostra casa abusiva all'interno del dipartimento: l'aula di Geologia Strutturale. Chi sono questi ragazzi? Chiara Anzolini, Matteo Demurtas, Alberto Ceccato e Laura, Luca Dal Zilio, Giacomo Pozzi, Francesca 'Frappe' Prando; poi, speciale menzione anche a Laura Busato per avermi sopportato per le continue richieste d'aiuto per LateX durante la stesura della relazione di Spiess. Ringrazio tutti gli amici che mi sono fatto a Padova in questi ultimi anni tra cui la Elena Lucietto (è sempre colpa sua), la Greta 'Meraviglia!', Enrico Boesso, Marco Boato [2] e tanti altri, poi ringrazio infinitamente i miei amici di Este, Diego Masiero [3], Filippo Lorenzin e Giuseppe di Nunno che rimangono sempre nel mio granitico cuore.
Infine, il penultimo ringraziamento, ma non di meno importante va alla mia famiglia, che oltre ad avermi sostenuto mi hanno guidato attraverso le peripezie del mondo rendendomi come sono ora. L'ultimo, invece, va ad una persona che mi ha dato il necessario coraggio di intraprendere un percorso universitario, ovvero la mia vecchia professoressa di matematica Maria Grazia Ceccato , la quale tramite il terrore e la severità mi ha fatto capire che non ero stupido come pensavo. Grazie infinite e di cuore.
Se nel frontespizio ho iniziato con una citazione di Guida Galattica per Autostoppisti, ora concludo con un'altra citazione, sempre facente parte di quel fantastico romanzo di fantascienza:
"So Long and thanks for all the fish" The Hitchhikers's Guide to the Galaxy, Douglas Adams

[2]Per gli aperitivi colmi d'amore e lamentazioni insieme a Moreno Clementi
[3]In particolare per il supporto grafico e linguistico datomi. Il supporto grafico è stato semplicemente -Ehi, Andrea, guarda che premendo shift e cliccando sull'immagine la rimpicciolisci senza modificare le proporzioni-

Bibliography

[Avouac and Burov, 1996] Avouac, J.-P. and Burov, E. (1996). Erosion as a driving mechanism of intracontinental mountain growth. *Journal of Geophysical Research: Solid Earth (1978–2012)*, 101(B8):17747–17769.

[Beaumont et al., 2010] Beaumont, C., Jamieson, R., and Nguyen, M. (2010). Models of large, hot orogens containing a collage of reworked and accreted terranes. *Canadian Journal of Earth Sciences*, 47(4):485–515.

[Beaumont et al., 2001] Beaumont, C., Jamieson, R. A., Nguyen, M., and Lee, B. (2001). Himalayan tectonics explained by extrusion of a low-viscosity crustal channel coupled to focused surface denudation. *Nature*, 414(6865):738–742.

[Beaumont et al., 2004] Beaumont, C., Jamieson, R. A., Nguyen, M. H., and Medvedev, S. (2004). Crustal channel flows: 1. numerical models with applications to the tectonics of the himalayan-tibetan orogen. *Journal of Geophysical Research: Solid Earth (1978–2012)*, 109(B6).

[Beaumont et al., 2006] Beaumont, C., Nguyen, M., Jamieson, R. A., and Ellis, S. (2006). Crustal flow modes in large hot orogens. *Geological Society, London, Special Publications*, 268(1):91–145.

[Bittner and Schmeling, 1995] Bittner, D. and Schmeling, H. (1995). Numerical modelling of melting processes and induced diapirism in the lower crust. *Geophysical Journal International*, 123(1):59–70.

[Burg and Gerya, 2005] Burg, J.-P. and Gerya, T. (2005). The role of viscous heating in barrovian metamorphism of collisional orogens: thermomechanical models and application to the lepontine dome in the central alps. *Journal of Metamorphic Geology*, 23(2):75–95.

[Burg and Schmalholz, 2008] Burg, J.-P. and Schmalholz, S. (2008). Viscous heating allows thrusting to overcome crustal-scale buckling: Numerical investigation with application to the himalayan syntaxes. *Earth and Planetary Science Letters*, 274(1):189–203.

[Burov et al., 2014] Burov, E., Francois, T., Yamato, P., and Wolf, S. (2014). Mechanisms of continental subduction and exhumation of hp and uhp rocks. *Gondwana Research*, 25(2):464–493.

[Burov and Toussaint, 2007] Burov, E. and Toussaint, G. (2007). Surface processes and tectonics: forcing of continental subduction and deep processes. *Global and Planetary Change*, 58(1):141–164.

[Caricchi et al., 2007] Caricchi, L., Burlini, L., Ulmer, P., Gerya, T., Vassalli, M., and Papale, P. (2007). Non-newtonian rheology of crystal-bearing magmas and implications for magma ascent dynamics. *Earth and Planetary Science Letters*, 264(3):402–419.

[Carosi et al., 2010] Carosi, R., Montomoli, C., Rubatto, D., and Visonà, D. (2010). Late oligocene high-temperature shear zones in the core of the higher himalayan crystallines (lower dolpo, western nepal). *Tectonics*, 29(4).

[Carosi et al., 2013] Carosi, R., Montomoli, C., Rubatto, D., and Visonà, D. (2013). Leucogranite intruding the south tibetan detachment in western nepal: implications for exhumation models in the himalayas. *Terra Nova*, 25(6):478–489.

[Chemenda et al., 2000] Chemenda, A. I., Burg, J.-P., and Mattauer, M. (2000). Evolutionary model of the himalaya–tibet system: geopoem: based on new modelling, geological and geophysical data. *Earth and Planetary Science Letters*, 174(3):397–409.

[Chen et al., 2013] Chen, L., Gerya, T., Zhang, Z., Zhu, G., Duretz, T., and Jacoby, W. R. (2013). Numerical modeling of eastern tibetan-type margin: influences of surface processes, lithospheric structure and crustal rheology. *Gondwana Research*, 24(3):1091–1107.

[Clauser and Huenges, 1995] Clauser, C. and Huenges, E. (1995). Thermal conductivity of rocks and minerals. *Rock physics & phase relations: A handbook of physical constants*, pages 105–126.

[Crameri et al., 2012] Crameri, F., Schmeling, H., Golabek, G., Duretz, T., Orendt, R., Buiter, S., May, D., Kaus, B., Gerya, T., and Tackley, P. (2012). A comparison of numerical surface topography calculations in geodynamic modelling: An evaluation of the 'sticky air'method. *Geophysical Journal International*, 189(1):38–54.

[De Smet et al., 2000] De Smet, J. H., Van Den Berg, A. P., Vlaar, N. J., and Yuen, D. A. (2000). A characteristics-based method for solving the transport equation and its application to the process of mantle differentiation and continental root growth. *Geophysical Journal International*, 140(3):651–659.

[Faccenda, 2014] Faccenda, M. (2014). Mid mantle seismic anisotropy around subduction zones. *Physics of the Earth and Planetary Interiors*, 227:1–19.

[Faccenda et al., 2008] Faccenda, M., Gerya, T. V., and Chakraborty, S. (2008). Styles of post-subduction collisional orogeny: influence of convergence velocity, crustal rheology and radiogenic heat production. *Lithos*, 103(1):257–287.

[Fornberg, 1998] Fornberg, B. (1998). *A practical guide to pseudospectral methods*, volume 1. Cambridge university press.

[Gerya, 2009] Gerya, T. (2009). *Introduction to numerical geodynamic modelling*. Cambridge University Press.

[Gerya et al., 2008] Gerya, T., Perchuk, L., and Burg, J.-P. (2008). Transient hot channels: perpetrating and regurgitating ultrahigh-pressure, high-temperature crust–mantle associations in collision belts. *Lithos*, 103(1):236–256.

[Gerya and Stöckhert, 2006] Gerya, T. and Stöckhert, B. (2006). Two-dimensional numerical modeling of tectonic and metamorphic histories at active continental margins. *International Journal of Earth Sciences*, 95(2):250–274.

[Gerya and Burg, 2007] Gerya, T. V. and Burg, J.-P. (2007). Intrusion of ultramafic magmatic bodies into the continental crust: numerical simulation. *Physics of the Earth and Planetary Interiors*, 160(2):124–142.

[Gerya and Yuen, 2003] Gerya, T. V. and Yuen, D. A. (2003). Characteristics-based marker-in-cell method with conservative finite-differences schemes for modeling geological flows with strongly variable transport properties. *Physics of the Earth and Planetary Interiors*, 140(4):293–318.

[Gerya and Yuen, 2007] Gerya, T. V. and Yuen, D. A. (2007). Robust characteristics method for modelling multiphase visco-elasto-plastic thermo-mechanical problems. *Physics of the Earth and Planetary Interiors*, 163(1):83–105.

[Grujic et al., 1996] Grujic, D., Casey, M., Davidson, C., Hollister, L. S., Kündig, R., Pavlis, T., and Schmid, S. (1996). Ductile extrusion of the higher himalayan crystalline in bhutan: evidence from quartz microfabrics. *Tectonophysics*, 260(1):21–43.

[He et al., 2014] He, D., Webb, A. A. G., Larson, K. P., Martin, A. J., and Schmitt, A. K. (2014). Extrusion vs. duplexing models of himalayan mountain building 3: duplexing dominates from the oligocene to present. *International Geology Review*, (ahead-of-print):1–27.

[Heim and Gansser, 1939] Heim, A. and Gansser, A. (1939). Central himalaya.

[Hertszprung, 1905] Hertszprung, E. (1905). Zure strahlung der stern. *Zeitschrift für wissenschaftliche Photographie*, 3:429–442.

[Hodges et al., 1992] Hodges, K., Parrish, R., Housh, T., Lux, D., Burchfiel, B., Royden, L., and Chen, Z. (1992). Simultaneous miocene extension and shortening in the himalayan orogen. *Science*, 258(5087):1466–1470.

[Imayama et al., 2012] Imayama, T., Takeshita, T., Yi, K., Cho, D.-L., Kitajima, K., Tsutsumi, Y., Kayama, M., Nishido, H., Okumura, T., Yagi, K., et al. (2012). Two-stage partial melting and contrasting cooling history within the higher himalayan crystalline sequence in the far-eastern nepal himalaya. *Lithos*, 134:1–22.

[Ismail-Zadeh and Tackley, 2010] Ismail-Zadeh, A. and Tackley, P. (2010). *Computational methods for geodynamics*. Cambridge University Press.

[Kohn, 2008] Kohn, M. J. (2008). Ptt data from central nepal support critical taper and repudiate large-scale channel flow of the greater himalayan sequence. *Geological Society of America Bulletin*, 120(3-4):259–273.

[Kumar et al., 2009] Kumar, P. S., Menon, R., and Reddy, G. (2009). Heat production heterogeneity of the indian crust beneath the himalaya: Insights from the northern indian shield. *Earth and Planetary Science Letters*, 283(1):190–196.

[Malevsky and Yuen, 1991] Malevsky, A. V. and Yuen, D. A. (1991). Characteristics-based methods applied to infinite prandtl number thermal convection in the hard turbulent regime. *Physics of Fluids A: Fluid Dynamics (1989-1993)*, 3(9):2105–2115.

[Mase and Mase, 2010] Mase, G. T. and Mase, G. E. (2010). *Continuum mechanics for engineers*. CRC press.

[Montomoli et al., 2014] Montomoli, C., Carosi, R., and Iaccarino, S. (2014). Tectonometamorphic discontinuities in the greater himalayan sequence: a local or a regional feature? *Geological Society, London, Special Publications*, 412:SP412–3.

[Montomoli et al., 2013] Montomoli, C., Iaccarino, S., Carosi, R., Langone, A., and Visona, D. (2013). Tectonometamorphic discontinuities within the greater himalayan sequence in western nepal (central himalaya): Insights on the exhumation of crystalline rocks. *Tectonophysics*, 608:1349–1370.

[Moresi et al., 2003] Moresi, L., Dufour, F., and Mühlhaus, H.-B. (2003). A lagrangian integration point finite element method for large deformation modeling of viscoelastic geomaterials. *Journal of Computational Physics*, 184(2):476–497.

[Nelson et al., 1996] Nelson, K. D., Zhao, W., Brown, L., Kuo, J., Che, J., Liu, X., Klemperer, S., Makovsky, Y., Meissner, R., Mechie, J., et al. (1996). Partially molten middle crust beneath southern tibet: synthesis of project indepth results. *Science*, 274(5293):1684–1688.

[Patankar, 1980] Patankar, S. (1980). *Numerical heat transfer and fluid flow*. CRC Press.

[Pinkerton and Stevenson, 1992] Pinkerton, H. and Stevenson, R. (1992). Methods of determining the rheological properties of magmas at sub-liquidus temperatures. *Journal of Volcanology and Geothermal Research*, 53(1):47–66.

[Ranalli, 1995] Ranalli, G. (1995). *Rheology of the Earth*. Springer.

[Rosenberg and Handy, 2005] Rosenberg, C. and Handy, M. (2005). Experimental deformation of partially melted granite revisited: implications for the continental crust. *Journal of metamorphic Geology*, 23(1):19–28.

[Russell, 1912] Russell, H. N. (1912). Relations between the spectra and other characteristics of the stars. *Proceedings of the American Philosophical Society*, pages 569–579.

[Thiede and Ehlers, 2013] Thiede, R. C. and Ehlers, T. A. (2013). Large spatial and temporal variations in himalayan denudation. *Earth and Planetary Science Letters*, 371:278–293.

[Toussaint et al., 2004] Toussaint, G., Burov, E., and Avouac, J.-P. (2004). Tectonic evolution of a continental collision zone: A thermomechanical numerical model. *Tectonics*, 23(6).

[Turcotte and Schubert, 2014] Turcotte, D. L. and Schubert, G. (2014). *Geodynamics*. Cambridge University Press.

[Vance et al., 2003] Vance, D., Bickle, M., Ivy-Ochs, S., and Kubik, P. W. (2003). Erosion and exhumation in the himalaya from cosmogenic isotope inventories of river sediments. *Earth and Planetary Science Letters*, 206(3):273–288.

[Vanderhaeghe, 2009] Vanderhaeghe, O. (2009). Migmatites, granites and orogeny: Flow modes of partially-molten rocks and magmas associated with melt/solid segregation in orogenic belts. *Tectonophysics*, 477(3):119–134.

[Vilà et al., 2010] Vilà, M., Fernández, M., and Jiménez-Munt, I. (2010). Radiogenic heat production variability of some common lithological groups and its significance to lithospheric thermal modeling. *Tectonophysics*, 490(3):152–164.

[Visona et al., 2012] Visona, D., Carosi, R., Montomoli, C., Tiepolo, M., and Peruzzo, L. (2012). Miocene andalusite leucogranite in central-east himalaya (everest–masang kang area): Low-pressure melting during heating. *Lithos*, 144:194–208.

[Webb et al., 2011] Webb, A. A. G., Schmitt, A. K., He, D., and Weigand, E. L. (2011). Structural and geochronological evidence for the leading edge of the greater himalayan crystalline complex in the central nepal himalaya. *Earth and Planetary Science Letters*, 304(3):483–495.

[Webb et al., 2007] Webb, A. A. G., Yin, A., Harrison, T. M., Célérier, J., and Burgess, W. P. (2007). The leading edge of the greater himalayan crystalline complex revealed in the nw indian himalaya: Implications for the evolution of the himalayan orogen. *Geology*, 35(10):955–958.

[Wibberley et al., 2008] Wibberley, C. A., Yielding, G., and Di Toro, G. (2008). Recent advances in the understanding of fault zone internal structure: a review. *Geological Society, London, Special Publications*, 299(1):5–33.

[Wintsch et al., 1995] Wintsch, R., Christoffersen, R., and Kronenberg, A. (1995). Fluid-rock reaction weakening of fault zones. *Journal of Geophysical Research: Solid Earth (1978–2012)*, 100(B7):13021–13032.

[Woidt, 1978] Woidt, W.-D. (1978). Finite element calculations applied to salt dome analysis. *Tectonophysics*, 50(2):369–386.

[Yin, 2006] Yin, A. (2006). Cenozoic tectonic evolution of the himalayan orogen as constrained by along-strike variation of structural geometry, exhumation history, and foreland sedimentation. *Earth Science Reviews*, 76:1–131.

[Yin and Harrison, 2000] Yin, A. and Harrison, T. M. (2000). Geologic evolution of the himalayan-tibetan orogen. *Annual Review of Earth and Planetary Sciences*, 28(1):211–280.

[Zhang et al., 2012] Zhang, J., Santosh, M., Wang, X., Guo, L., Yang, X., and Zhang, B. (2012). Tectonics of the northern himalaya since the india–asia collision. *Gondwana Research*, 21(4):939–960.